The Hawaii Infrared Parallax Program. V. New T-Dwarf Members and Candidate Members of Nearby Young Moving Groups

DRAFT VERSION FEBRUARY 11, 2021
Typeset using LaTeX **twocolumn** style in AASTeX61

The Hawaii Infrared Parallax Program. V. New T-Dwarf Members and Candidate Members of Nearby Young Moving Groups

ZHOUJIAN ZHANG (张周健),[1] MICHAEL C. LIU,[1] WILLIAM M. J. BEST,[2] TRENT J. DUPUY,[3,4] AND ROBERT J. SIVERD[3]

[1]*Institute for Astronomy, University of Hawaii at Manoa, Honolulu, HI 96822, USA*
[2]*The University of Texas at Austin, Department of Astronomy, 2515 Speedway, C1400, Austin, TX 78712, USA*
[3]*Gemini Observatory/NSF's NOIRLab, 670 N. A'ohoku Place, Hilo, HI, 96720, USA*
[4]*Institute for Astronomy, University of Edinburgh, Royal Observatory, Blackford Hill, Edinburgh, EH9 3HJ, UK*

(Received Nov 5, 2020; Revised Feb 4, 2021; Accepted Feb 5, 2021)

Submitted to ApJ

ABSTRACT

We present a search for new planetary-mass members of nearby young moving groups (YMGs) using astrometry for 694 T and Y dwarfs, including 447 objects with parallaxes, mostly produced by recent large parallax programs from UKIRT and *Spitzer*. Using the BANYAN Σ and LACEwING algorithms, we identify 30 new candidate YMG members, with spectral types of T0−T9 and distances of 10 − 43 pc. Some candidates have unusually red colors and/or faint absolute magnitudes compared to field dwarfs with similar spectral types, providing supporting evidence for their youth, including 4 early-T dwarfs. We establish one of these, the variable T1.5 dwarf 2MASS J21392676+0220226, as a new planetary-mass member ($14.6^{+3.2}_{-1.6}$ M_{Jup}) of the Carina-Near group (200 ± 50 Myr) based on its full six-dimensional kinematics, including a new parallax measurement from CFHT. The high-amplitude variability of this object is suggestive of a young age, given the coexistence of variability and youth seen in previously known YMG T dwarfs. Our four latest-type (T8−T9) YMG candidates, WISE J031624.35 + 430709.1, ULAS J130217.21 + 130851.2, WISEPC J225540.74 − 311841.8, and WISE J233226.49 − 432510.6, if confirmed, will be the first free-floating planets (≈ 2 − 6 M_{Jup}) whose ages and luminosities are compatible with both hot-start and cold-start evolutionary models, and thus overlap the properties of the directly-imaged planet 51 Eri b. Several of our early/mid-T candidates have peculiar near-infrared spectra, indicative of heterogenous photospheres or unresolved binarity. Radial velocity measurements needed for final membership assessment for most of our candidates await upcoming 20–30 meter class telescopes. In addition, we compile all 15 known T7−Y1 benchmarks and derive a homogeneous set of their effective temperatures, surface gravities, radii, and masses.

1. INTRODUCTION

A plethora of planetary-mass objects have been discovered beyond our solar system in the past 25 years. Among these objects, gas-giant planets (≈ 1 − 13 M_{Jup}) that are either wide-separation companions to stars or brown dwarfs (e.g., Goldman et al. 2010; Naud et al. 2014; Miles-Páez et al. 2017; Dupuy et al. 2018) or free-floating objects (e.g., Liu et al. 2013; Best et al. 2017; Schneider et al. 2017; Zhang et al. 2018) are a valuable subset for high-quality emission spectroscopy, given the lack of the contaminating light from host stars. These objects thereby serve as excellent laboratories to study self-luminous exoplanet atmospheres, as well as exoplanet formation and evolution. As they are too low in mass to fuse either hydrogen or deuterium in their cores, planetary-mass objects contract, cool, and fade after their initial formation (e.g., Burrows et al. 2001; Marley et al. 2007). Consequently, searches for self-luminous giant planets have focused on the nearest young (≈ 10 − 200 Myr) moving groups (YMGs) and stellar associations, where planetary-mass objects are bright enough to be directly detected. Moreover, by virtue of their shared membership, these planetary-mass objects can adopt the age estimates inferred for the stellar members of the same groups, making them "age benchmarks" (e.g., Pinfield et al. 2006; Liu et al. 2007) for testing models of substellar evolution and ultracool atmospheres.

Substantial progress has been made to identify new members of nearby YMGs and has spawned a variety of methods for membership assessment (e.g., Zuckerman et al. 2004; Mamajek 2005; Torres et al. 2006; Shkolnik et al. 2012; Malo et al. 2013; Bowler et al. 2017, 2019; Riedel et al. 2017;

Gagné et al. 2018b; Crundall et al. 2019). These methods rely on the objects' space motions to establish membership, along with spectrophotometric evidence to establish their youthfulness. With precise proper motions and parallaxes, *Gaia* DR2 (Gaia Collaboration et al. 2016, 2018) has enabled kinematic studies of the solar neighborhood and greatly expanded the stellar and substellar census of nearby associations (e.g., Gagné & Faherty 2018). However, optical data from *Gaia* are not sensitive to planetary-mass objects, whose spectral energy distributions peak at longer wavelengths. Deep optical and near-infrared sky surveys are valuable resources to find free-floating planets, including Pan-STARRS1 (PS1; Chambers et al. 2016), UKIDSS (Lawrence et al. 2007, 2012), and the *WISE* surveys (Wright et al. 2010; Cutri 2014; Eisenhardt et al. 2020; Marocco et al. 2020). These catalogs provide proper motions, but parallaxes are either lacking or low-accuracy given the limited number of epochs and time baseline, thus inhibiting the identification of new association members.

Given these challenges, the current planetary-mass census of nearby associations is largely incomplete and has a significant deficit at T and Y spectral types. Mid- to late-T dwarfs are among the most common field population in the solar neighborhood (e.g., Kirkpatrick et al. 2012; Burningham et al. 2013; Marocco et al. 2015; Best et al. 2021), but we still have limited census of such objects at young ages. Only a handful of T-dwarf (and no Y-dwarf) YMG members have been found to date (Naud et al. 2014; Macintosh et al. 2015; Gagné et al. 2015, 2017, 2018a), and a larger sample of such objects is needed to investigate their atmospheres ($T_{\rm eff} \approx 500-1200$ K) at low surface gravities.

The recent completion of infrared parallax programs by Kirkpatrick et al. (2019) and by Best et al. (2020a) has provided the largest batch (over 300 objects) of new proper motions and parallaxes for LTY-type ultracool dwarfs, and these precise data open the door to a large-scale search for late-type YMG members. In this work, we combine available astrometry and radial velocities of 694 T and Y dwarfs (447 objects with parallaxes) to identify new and candidate members of nearby YMGs (Section 2). By studying the astrometric, photometric, and spectroscopic properties of our candidates, we have confirmed a new planetary-mass member in the Carina-Near moving group and found 29 other T-dwarf candidate members, including several with unusual spectrophotometric properties (Section 3). Finally, we provide a summary and discuss future follow-up of our candidates (Section 4).

2. IDENTIFICATION OF NEW YOUNG MOVING GROUP MEMBERS

2.1. *Data*

We start our analysis using The UltracoolSheet[1] (Best et al. 2020b), a catalog of astrometry, photometry, spectroscopy, and multiplicity for over 3,000 ultracool dwarfs and imaged exoplanets. Developed from compilations of ultracool dwarfs by Dupuy & Liu (2012), Dupuy & Kraus (2013), Liu et al. (2016), Best et al. (2018), and Best et al. (2021), The UltracoolSheet is complete for all spectroscopically confirmed objects with $\geqslant$L0 spectral types known prior to April 15, 2015 and is further augmented by new ultracool dwarfs discovered by Best et al. (2015, 2017) and all imaged exoplanets discovered since then. Sky positions, proper motions, parallaxes, and radial velocities of objects in The UltracoolSheet are compiled from numerous catalogs, including *Gaia* DR2 (Gaia Collaboration et al. 2016, 2018), PS1 (Chambers et al. 2016), UKIDSS (Lawrence et al. 2007, 2012), AllWISE (Cutri 2014), the SIMBAD Astronomical Database (Wenger et al. 2000), and recent large near-infrared parallax programs by Dahn et al. (2017), Smart et al. (2018), Kirkpatrick et al. (2019), and Best et al. (2020a).

For one particular T dwarf, 2MASS J21392676+0220226 (2MASS J2139+0220), we also include our new astrometry measurements. We monitored this object with the facility infrared camera WIRCam (Puget et al. 2004) on the Canada-France-Hawaii Telescope (CFHT) from 2012–2017. Using 5-second exposures in the J band, we achieved signal-to-noise ratios (S/Ns) of $90-160$ on the target in individual frames, obtaining an average of 18 frames per epoch, from which we measured the (x,y) positions of it and 126 reference stars. Using our custom pipeline (Dupuy & Liu 2012; Dupuy et al. 2015), we reduced these individual measurements into high-precision multi-epoch relative astrometry, with the absolute calibration provided by 91 low-proper-motion 2MASS stars (Cutri et al. 2003). We derived the relative parallax and proper motion for 2MASS J2139+0220 using our standard MCMC approach and then, in order to be consistent with our many previously published CFHT parallaxes, converted to an absolute reference frame using the Besançon galaxy model to simulate the distances of the reference stars (Robin et al. 2003). Our thirteen epochs of astrometry spanning 4.94 years yield an absolute parallax of 96.5 ± 1.1 mas and proper motion of $(489.7\pm0.7, 125.0\pm0.8)$ mas yr^{-1}. We found a very reasonable reduced $\chi^2=1.04$ for our best-fit solution with 21 degrees of freedom (Figure 1).

Multiple astrometric and kinematic measurements for the same objects in The UltracoolSheet are unified following the approach described below (see Best et al. 2020b for more details). For objects that are companions in binary systems, we assume the companion has the same sky position, proper mo-

[1] http://bit.ly/UltracoolSheet

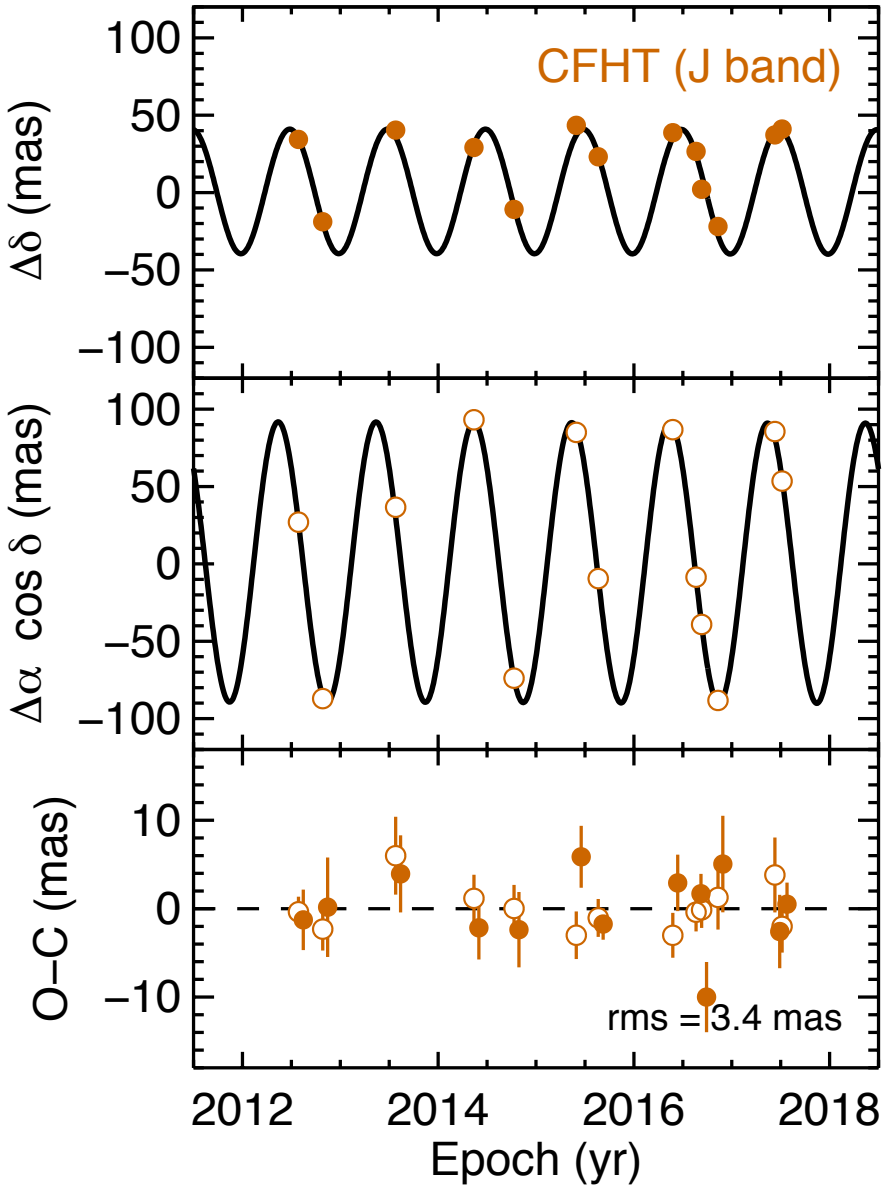

Figure 1. Relative astrometry of 2MASS J2139 + 0220 from CFHT/WIRCam. In the top two panels, the best-fit proper motions have been subtracted (for display purposes only), and the best-fit parallax solution is plotted as a solid black line. The bottom panel shows the residuals about the best-fit solution, with small x-axis offsets added to the $\Delta\delta$ residuals to more clearly show error bars. Our best-fit solution has a reduced $\chi^2 = 1.04$ with 21 degrees of freedom.

tion, and parallax as its host stars if (1) this binary system has an angular separation of $\leqslant 1''$, or (2) the companion has no direct astrometry from the existing catalogs. We also adopt the host stars' radial velocities if these values are lacking or have lower precision for the companions.

We computed J2000 sky positions of all ultracool dwarfs using the following preferences (from highest to lowest): *Gaia* DR2, PS1, UKIDSS, AllWISE, and SIMBAD. The coordinates of PS1 and UKIDSS are given at the observed epoch, so we computed J2000 coordinates using the reported epochs and proper motions. Such calculation is also performed by SIMBAD for *Gaia* DR2.

The final adopted proper motions and parallaxes of ultracool dwarfs are taken from *Gaia* DR2 if available and otherwise from the most precise measurements among PS1 and the literature. The objects' PS1 parallaxes are required to have the S/N of at least 5. We allow the adopted proper motions and parallaxes of a given object to come from different

references. The radial velocities are mostly obtained from SIMBAD, available for nearly 1,000 objects.

We identify new members and candidate members of nearby YMGs by using the resulting compilation of astrometry and radial velocities of 694 T and Y dwarfs in The UltracoolSheet (447 objects with parallaxes), including both single objects and components of resolved binary/multiple systems. For objects without trigonometric parallaxes, we use the photometric distances available in The UltracoolSheet, with final values calculated from $W2$, K, or J band[2]. Photometric distances are computed using the Dupuy & Liu (2012) relation between absolute magnitudes and spectral types established for field-age, high-gravity objects. This relation differs for young, low-gravity objects, especially at the L/T transition (e.g., Liu et al. 2013, 2016; Faherty et al. 2016; Zhang et al. 2020a), so we treat with caution candidate YMG members identified using photometric distances.

2.2. *Membership Assessment*

We use both BANYAN Σ (version 1.2; Gagné et al. 2018b) and LACEwING (Riedel et al. 2017) to evaluate whether a given object in The UltracoolSheet is a YMG member. BANYAN Σ is a Bayesian inference framework that compares an object's sky position and proper motion (as well as its parallax and radial velocity when available) to those of bona fide members of 29 young moving groups and associations ($\approx 1-800$ Myr) within 150 pc and field stars simulated by the Besançon Galactic model (Robin et al. 2003), and then computes a membership probability based on the object's Galactic coordinates and space velocity ($XYZUVW$). A threshold value for the computed Bayesian probabilities is needed to assess the objects' membership and the robustness of such a threshold can be tested against known YMG members and synthetic field stars, with the results described by the confusion matrix and derived quantities, including the true-positive rate (i.e., the fraction of known members recovered) and false-positive rate (i.e., the fraction of contaminating field stars that are incorrectly classified as members). In principle, different probability thresholds are needed for different associations in order to achieve the same recovery/contamination rate, given that the YMGs have a variety of sizes, distances, and membership completeness. To reduce such association dependence for the threshold, Gagné et al. (2018b) customized their Bayesian priors and designed BANYAN Σ to produce similar recovery rates[3] for all 29 YMGs at a 90% threshold value. Therefore, the 90% probability reported by BANYAN Σ is not a metric for the true membership, but rather a value chosen to allow the classification performance among different YMGs to converge (see Section 7 of Gagné et al. 2018b).

LACEwING is a frequentist inference framework that compares an object's kinematics with those of nearby YMGs using the observed quantities (sky position, proper motion, parallax, radial velocity) rather than $XYZUVW$ as done by BANYAN Σ. LACEwING incorporates 16 young moving groups and associations ($\approx 5-800$ Myr) within 100 pc, which are all included in BANYAN Σ but with slightly different lists of bona fide members. The resulting LACEwING probability directly describes the likelihood that a given object is a kinematic member in each YMG, and the probabilities among all YMGs do not necessarily add up to 100% by design. Riedel et al. (2017) suggested probability thresholds of 66%, 40%, and 20% to select high-, moderate-, and low-probability candidate members, respectively. Unlike BANYAN Σ, a given probability threshold does not promise the similar recovery rate or contamination rate among different YMGs. Also, within the same YMG, any (positive) probability threshold can lead to a very wide range of recovery rates (spanning $0\%-100\%$) depending on the number and type of input astrometric parameters (e.g., see Figure 4 in Riedel et al. 2017).

We feed sky positions, proper motions, parallaxes, and radial velocities of The UltracoolSheet objects into BANYAN Σ and LACEwING, and then select T and Y dwarfs with $\geqslant 80\%$ BANYAN Σ or $\geqslant 66\%$ LACEwING membership probabilities. For BANYAN Σ, our chosen threshold will lead to a higher recovery rate of known YMG members than using 90%, with the specific enhancement depending on associations (see Figure 12 of Gagné et al. 2018b), but false-positive rates will increase as well. Using the BANYAN Σ and LACEwING results, we recover all the 5 T-dwarf YMG members known to date and find 30 new T-type candidate members[4] (Table 1). In the following section, we study the

[2] We adopt the objects' $W2$-based distances if their *WISE* photometry exists and is not contaminated by nearby sources (i.e., "nb == 1"). Otherwise, we adopt photometric distances computed from K_{2MASS} (more preferred) or K_{MKO} band for <T4.5 dwarfs, and from J_{2MASS} (more preferred) or J_{MKO} band for later-type objects.

[3] With the 90% probability threshold, BANYAN Σ can recover 50% (proper motion only), 68% (proper motion and radial velocity), 82% (proper motion and parallax), and 90% (proper motion, radial velocity, and parallax) of bona fide members of all associations (Gagné et al. 2018b). The false-positive rates for different associations depend on their angular sizes and characteristic kinematics but are usually $\leqslant 10^{-3}$.

[4] One of our candidate members, CFHT-Hy-20 (T2.5), was previously suggested as a Hyades member by Bouvier et al. (2008) based on the photometry and proper motion. The more precise proper motion, as well as the new parallax, measured by Liu et al. (2016) supported the object's Hyades membership. Here we also identify this object as a candidate, but do not consider it to be confirmed, given that a radial velocity measurement is lacking. In addition, while this paper was under review, new astrometry of 5 YMG candidates and 1 previously known YMG member became available from Kirkpatrick et al. (2020), which does not alter these objects' candidacy but does lead to slightly different membership probabilities (see footnote *b* of Table 1). Also, two other objects (WISE J033651.90+282628.8 and PSO J319.3102−29.6682) were previously considered as candidates but

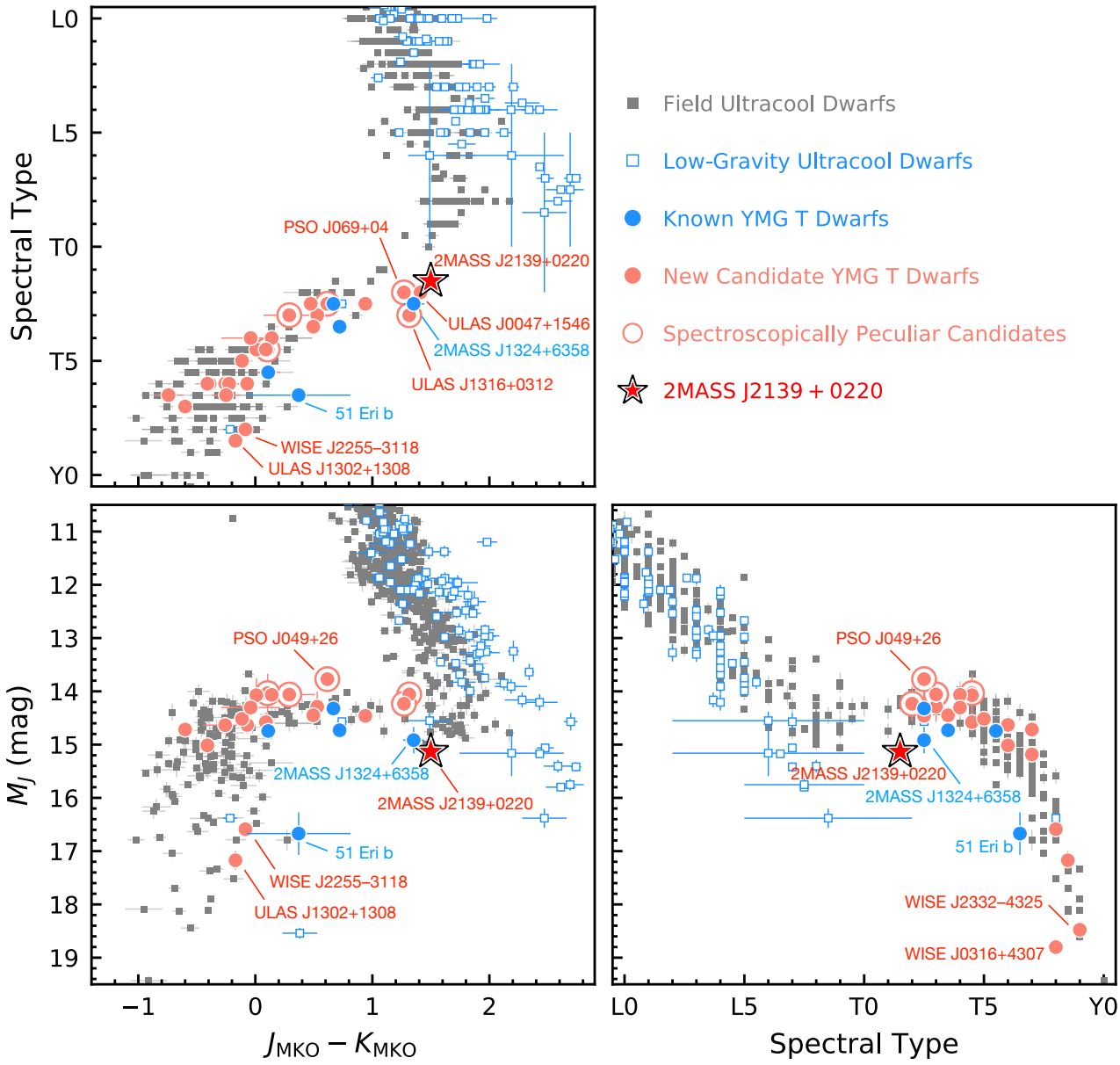

Figure 2. Near-infrared photometry of our newly confirmed Carina-Near member 2MASS J2139 + 0220 (red star), our newly identified YMG candidate members (light red circles), and recovered previously known T-dwarf YMG members (blue circles). We use open red circles to mark 7 YMG candidates with peculiar spectra indicative of either atmospheric variability or unresolved binarity (Section 3.2). Gray squares show known field dwarfs from The UltracoolSheet that have absolute magnitudes with S/N>5 and are not young, resolved binaries, or subdwarfs. Blue open squares show low-gravity L and T dwarfs in the field or YMGs.

photometric, spectroscopic, and physical properties of our candidates and discuss their membership.

3. PROPERTIES OF CANDIDATE MEMBERS

3.1. *Photometric Properties*

Figure 2 and Table 2 present near-infrared photometry of our YMG candidates. Several early-T dwarfs exhibit ≈ 0.8 mag redder $J - K$ colors than field dwarfs with similar spectral types, including four of our candidate members, 2MASS J2139 + 0220 (T1.5), ULAS J004757.41 + 154641.4 (ULAS J0047 + 1546; T2), PSO J069.7303 + 04.3834 (PSO J069 + 04; T2), and ULAS J131610.13 + 031205.5 (ULAS J1316 + 0312; T3), as well as one previously

are now excluded from our analysis, since their YMG membership probabilities do not pass our criteria by using these objects' new and more precise astrometry from Kirkpatrick et al. (2020).

known AB Doradus member identified by Gagné et al. (2018a), 2MASS J13243553 + 6358281 (2MASS J1324 + 6358; T2.5). Also, both 2MASS J2139 + 0220 and 2MASS J1324 + 6358 have ≈ 0.6 mag fainter J-band absolute magnitudes than the field sequence. The anomalous photometry of these objects provides evidence for their youth, given that the L/T transition of ultracool dwarfs is surface-gravity dependent, with young, lower-gravity objects having fainter, redder near-infrared photometry than their older, higher-gravity counterparts at the same spectral type (e.g., Metchev & Hillenbrand 2006; Barman et al. 2011; Faherty et al. 2016; Liu et al. 2016).

The gravity dependence of the L/T transition likely diminishes from early to later T types (Zhang et al. 2020a). Therefore the membership of our remaining candidates, whose photometry follows the field sequence, is still plausible. Despite this, two of our late-T candidate members, WISEPC J225540.74 − 311841.8 (WISE J2255 − 3118; T8) and ULAS J130217.21 + 130851.2 (ULAS J1302 + 1308; T8.5), as well as one previously known β Pictoris member, 51 Eri b (T6.5; Macintosh et al. 2015), have redder $J-K$ colors than field dwarfs by 0.4 − 0.8 mag. Also, both WISE J031624.35 + 430709.1 (WISE J0316 + 4307; T8) and 51 Eri b have fainter J-band absolute magnitudes than the field sequence by 1.6 − 2.2 mag. These three late-T candidates are therefore likely young as well given their similar photometry to 51 Eri b.

3.2. *Spectroscopic Properties*

Among our 30 candidate YMG members, 20 objects have low-resolution ($R \sim 100$) near-infrared (0.8 − 2.5 μm) spectra observed by the NASA Infrared Telescope Facility (IRTF) with the facility spectrograph SpeX (Rayner et al. 2003) in prism mode. Here we investigate if any candidates exhibit spectral peculiarity, which is indicative of atmospheric variability or unresolved binarity, with the former related to the rotation of ultracool dwarfs with inhomogeneous photospheric condensate clouds (e.g., Radigan et al. 2014) and/or temperature fluctuations (e.g., Tremblin et al. 2020). In both the variability and binary scenarios, a peculiar spectrum might be described by the composite of two (parts of) photospheres with different effective temperatures. Therefore, empirical spectral indices designed to identify unresolved binaries (e.g., Burgasser et al. 2010a; Bardalez Gagliuffi et al. 2014) can also find objects with high-amplitude photometric variability (e.g., Radigan et al. 2012; Khandrika et al. 2013; Heinze et al. 2015; Yang et al. 2016; Manjavacas et al. 2019).

We have visually compared the IRTF/SpeX spectra of our 20 candidates to spectral standards from Burgasser et al. (2006) and Cushing et al. (2011) to identify any spectral peculiarity. We have also computed the Burgasser et al. (2010a) quantitative spectral indices to identify objects with spectra indicative of composite photospheres or unresolved binarity. As a result, we find 4 "strong" composite candidates, meeting at least 3 out of 6 Burgasser et al. (2010a) criteria (with updates by Bardalez Gagliuffi et al. 2015): PSO J069.7303 + 04.3834 (PSO J069 + 04; T2), PSO J049.1159 + 26.8409 (PSO J049 + 26; T2.5), PSO J168.1800 − 27.2264 (PSO J168 − 27; T2.5), and ULAS J1316 + 0312 (T3). We also find 6 "weak" composite candidates, meeting 1 − 2 criteria: 2MASS J2139 + 0220 (T1.5), CFHT-Hy-20 (T2.5), SDSS J152103.24 + 013142.7 (SDSS J1521 + 0131; T3), 2MASS J00132229 − 1143006 (2MASS J0013 − 1143; T4), WISEPA J081958.05 − 033529.0 (WISE J0819 − 0335; T4), and WISE J163645.56 − 074325.1 (WISE J1636 − 0743; T4.5). Such spectral peculiarity for 4 out of these 10 candidates has also been noted by Burgasser et al. (2010a), Best et al. (2015), and Kellogg et al. (2017) using the same criteria. We note that all 10 of our composite candidates reside in the L/T transition, with spectral types of T1.5–T4.5.

We further perform spectral decomposition for our 10 candidates with peculiar spectra following the method described in Burgasser et al. (2010a). We first construct empirical spectral templates by compiling all published IRTF/SpeX spectra of L5–T9 objects in The UltracoolSheet (most of which are obtained from the SpeX Prism Library; Burgasser 2014). We select objects that have median spectral S/N $\geqslant$ 30 per pixel in J band, as well as $K_{\rm MKO}$ magnitudes and parallaxes. We also exclude subdwarfs, resolved binaries, likely unresolved binaries identified in literature (using the same quantitative spectral indices as in this work), and all our identified YMG candidate members, leading to a total of 193 SpeX templates. We flux-calibrate each template using its $K_{\rm MKO}$-band absolute magnitude, with the WFCAM K-band filter and the corresponding zero-point flux from Hewett et al. (2006) and Lawrence et al. (2007), respectively. This step is different from Burgasser et al. (2010a), who estimated absolute magnitudes from spectral types using empirical relations. We then combine all possible pairs of flux-calibrated templates, resulting in 18,528 composite spectral templates. For the secondary component of each composite system, we further allow its absolute $K_{\rm MKO}$ magnitude to vary by 7 steps of 0 mag, ±0.2 mag, ±0.4 mag, and ±0.6 mag, use these magnitudes to flux-calibrate its spectrum again, and then generate 7 new composite spectral templates. These magnitude variations are chosen to account for the intrinsic $K_{\rm MKO}$-band photometric scatter of ultracool dwarfs at a given spectral types (e.g., Figure 25 of Dupuy & Liu 2012). We therefore obtain 129,696 composite spectral templates, expanded from the original set by a factor of 7. For a given binary candidate, we compare its spectrum with each composite template over wavelengths of 0.95 − 1.35 μm, 1.45 − 1.8 μm, and 2.0 − 2.35 μm, and then compute the flux scale factor

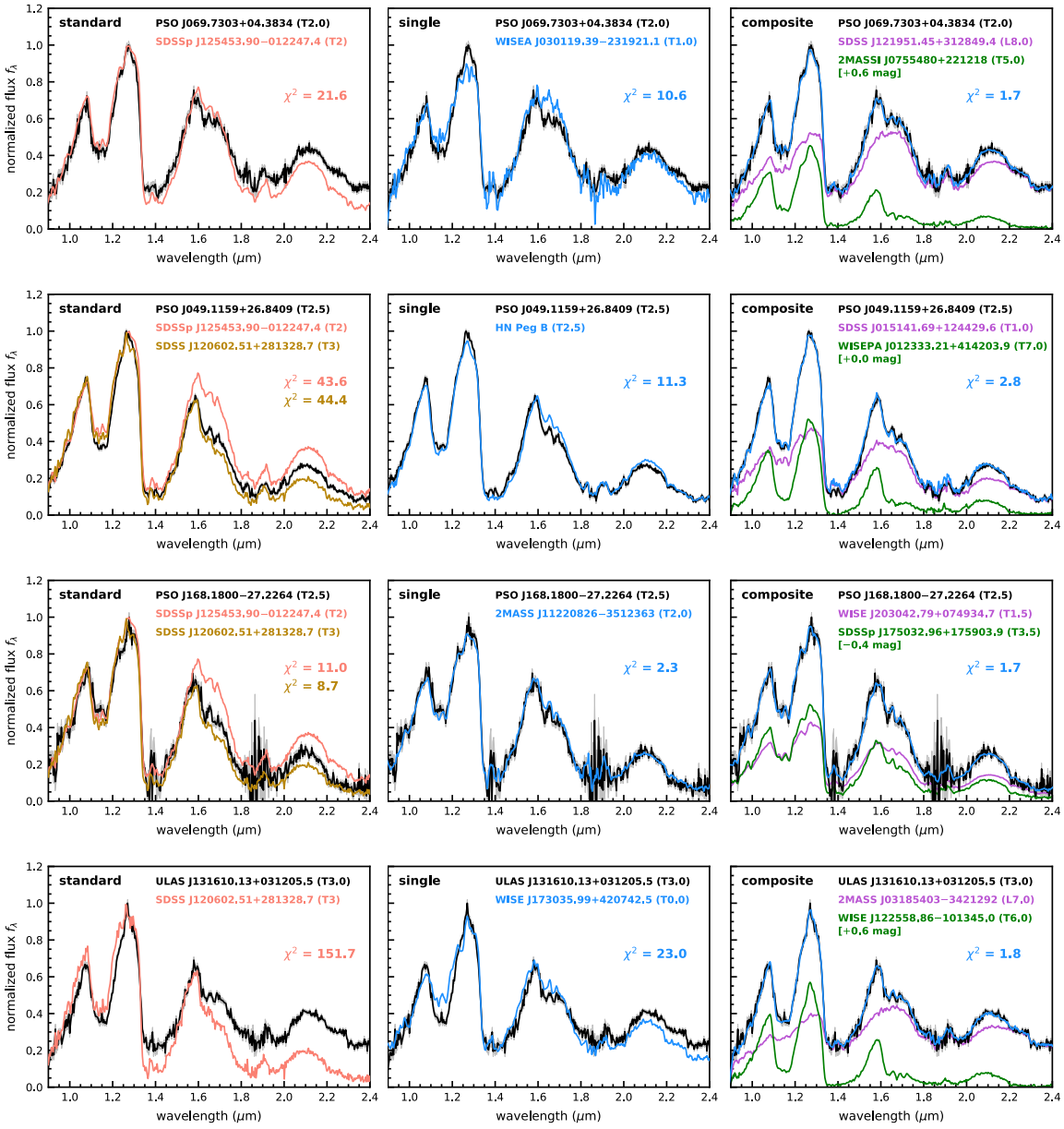

Figure 3. Near-infrared spectra of our 4 strong composite candidates, compared with spectral standards (left), the best-fit single-object spectral template (middle), and the best-fit composite spectral template (right), with χ^2 values labeled. In the left panel for each object, we show only one spectral standard if the object has an integer spectral type and two standards for objects with half types. In the right panel, we use purple and green for the primary and the secondary components, respectively, with the composite spectra shown in blue. The value in the brackets (green) indicates the magnitude offset we have added to the absolute $K_{\rm MKO}$ of the secondary when flux-calibrating its spectrum and generating the composite spectral template.

that minimizes the χ^2 (Equation 1 of Burgasser et al. 2010a). In addition to this synthetic composite fitting, we also fit the single-object spectral templates to our candidates' spectra with the same method. We have in total 246 single templates for such analysis as we do not require them to have parallaxes or $K_{\rm MKO}$ magnitudes. The best-fit single and composite templates for our 4 strong and 6 weak composite candidates are shown in Figures 3 and 4, respectively.

We do not quantitatively assess whether composite templates provide better spectral matches than the single-object ones for our objects. Instead, we visually examine the best-fit single and composite templates to study the spectral peculiarity of each candidate. We find the best-fit single-object templates of 6 candidates do not match their observed spectra, 2MASS J0013 − 1143, PSO J049 + 26, PSO J069 + 04, ULAS J1316 + 0312, WISE J1636 − 0743,

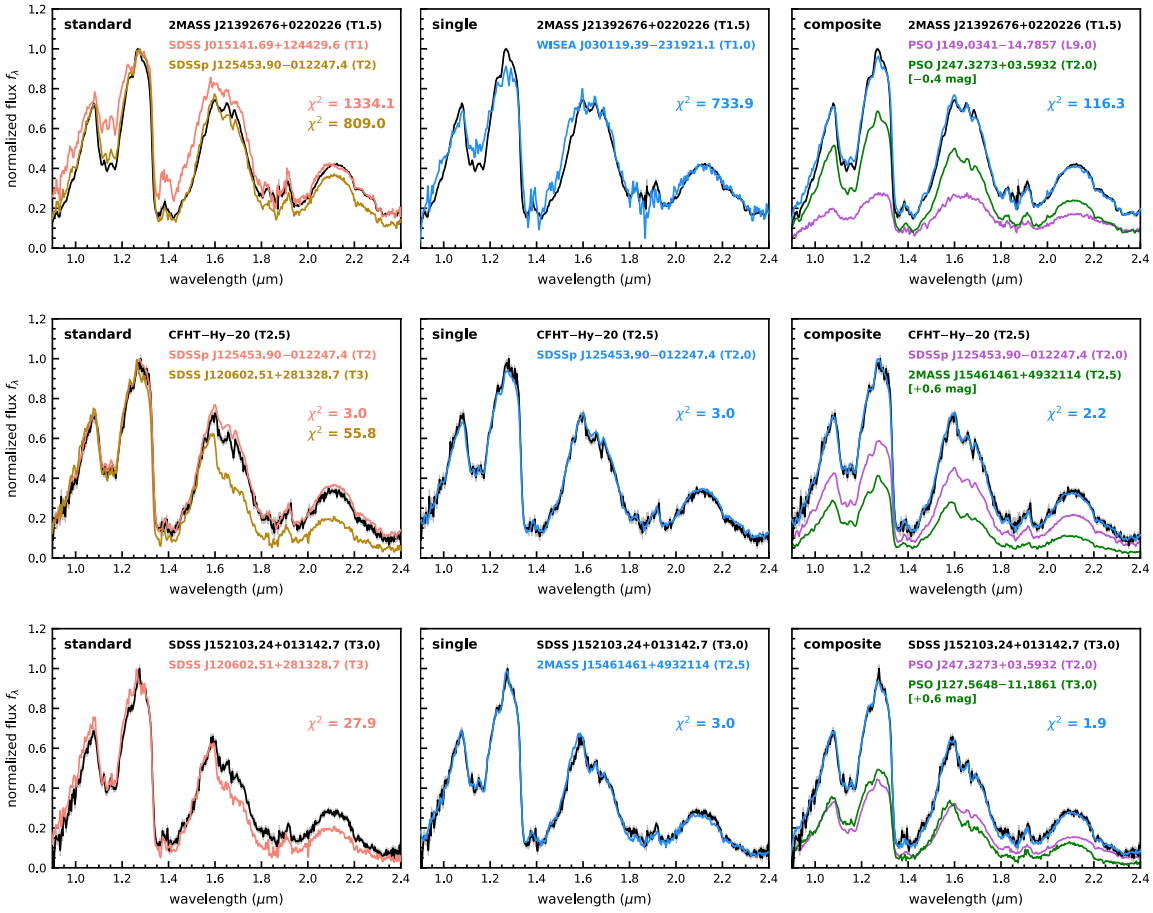

Figure 4. Near-infrared spectra of our 6 weak composite candidates with the same format as Figure 3.

and 2MASS J2139 + 0220. These objects have (1) stronger CH_4 absorption at 1.6 μm relative to 2.2 μm (PSO J049 + 26 and PSO J069 + 04), (2) more prominent *J*-band peakS and/or deeper H_2O and CH_4 absorption around 1.1 μm (2MASS J0013 − 1143, PSO J069 + 04, ULAS J1316 + 0312, WISE J1636 − 0743, 2MASS J2139 + 0220), or (3) less prominent blue wingS of *Y* band (2MASS J0013 − 1143 and 2MASS J2139 + 0220). The first two phenomena have also been seen in the integrated IRTF/SpeX spectra of binaries by Burgasser et al. (2010a). These differences do not appear when examining the best-fit composite templates of these 6 candidates. For the remaining 4 composite candidates, we do not see significant improvements by switching from single-object to composite spectral fitting.

Besides the 20 candidate YMG members with IRTF/SpeX spectra, our remaining 10 candidates have spectra taken by a variety of other instruments (Chiu et al. 2006; Pinfield et al. 2008; Burningham et al. 2010a; Albert et al. 2011; Kirkpatrick et al. 2012; Burningham et al. 2013; Day-Jones et al. 2013; Mace et al. 2013a), including UKIRT/UIST, UKIRT/CGS4, VLT/X-shooter, Subaru/ICRS, Gemini/NIRI, and Keck/NIRSPEC. Most of these spectra have only partial wavelength coverage in the near-infrared (e.g., *JH*-band only) and spectroscopic follow-up is needed to obtain spectra with wider, contiguous wavelength coverage for detailed atmospheric analysis. Among these 10 objects, only ULAS J0047 + 1436 has been flagged as a strong binary candidate, by Day-Jones et al. (2013) based on VLT/X-Shooter spectra and the Burgasser et al. (2010a) spectral index criteria. Day-Jones et al. (2013) also conducted spectral decomposition using templates from the SpeX Prism Library and found this object is well-fitted by a L8+T7 composite.

Among our 30 candidate YMG members, photometric variability has been reported for two objects, 2MASS J0013 − 1143 and 2MASS J2139 + 0220. 2MASS J0013 − 1143 has a peak-to-peak amplitude of 4.6 ± 0.2% in *J* band (Eriksson et al. 2019a). 2MASS J2139 + 0220 is the most variable ultracool dwarf known to date, with a peak-to-peak amplitude of 26 ± 1% in *J* band (Radigan et al. 2012) and 11 − 12% in *Spitzer*/IRAC [3.6] and [4.5] bands (Yang et al. 2016; Vos et al. 2017). Therefore, the unusual spectral features of these two objects are likely related to their vari-

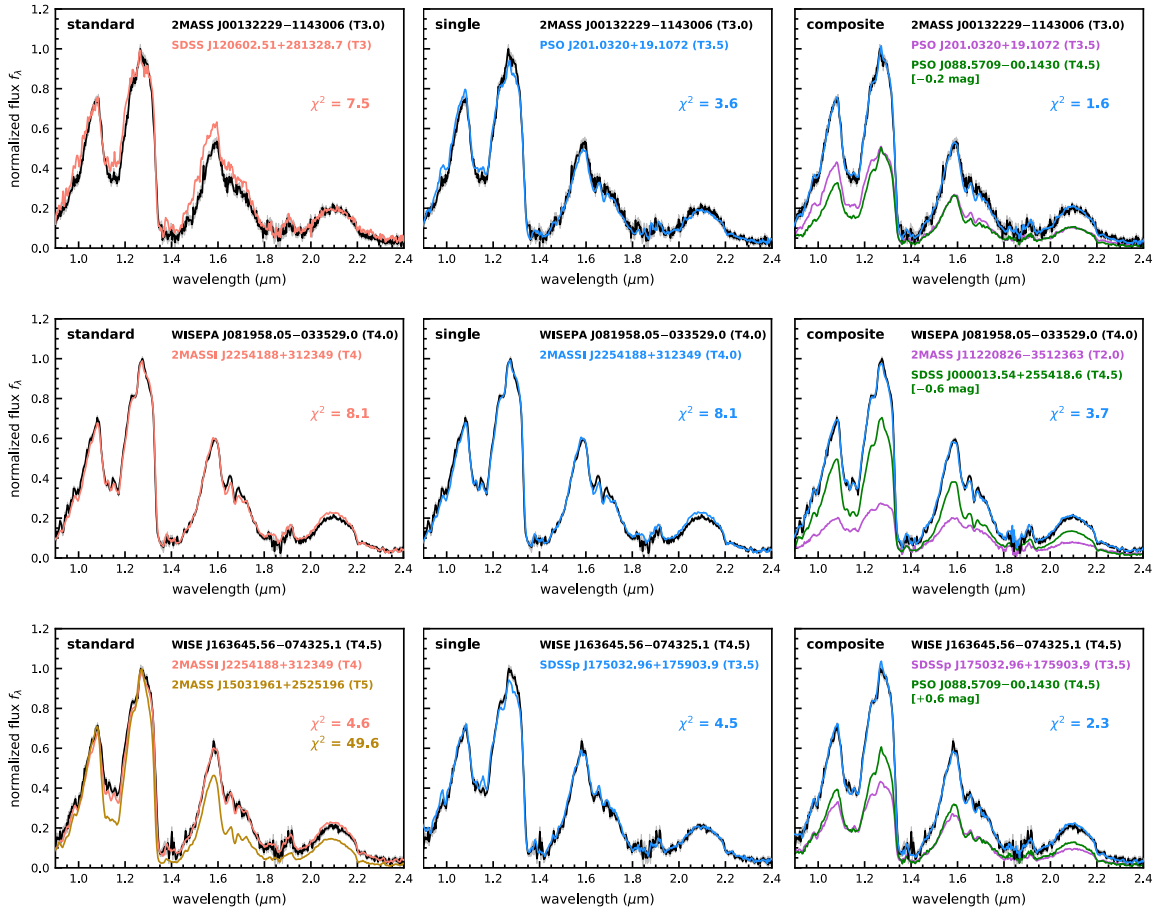

Figure 4. Continued

ability. Variability monitoring for all our remaining composite candidates would be helpful to further investigate these objects' spectral peculiarity. To summarize, we have identified a total of 7 T1.5–T4.5 candidates with peculiar spectra indicative of either atmospheric variability or unresolved binarity: 2MASS J0013 − 1143, PSO J049 + 26, PSO J069 + 04, ULAS J1316 + 0312, WISE J1636 − 0743, 2MASS J2139 + 0220, and ULAS J0047 + 1436 (Table 3).

3.3. *Physical Properties*

We derive physical properties of our 30 candidates by assuming they are all YMG members. We first estimate the objects' bolometric luminosities from their broadband photometry. There are 19 objects with T0−T7 spectral types and parallaxes, and 12 of them have K_{2MASS}, which we convert into L_{bol} using the Filippazzo et al. (2015) bolometric correction for young ultracool dwarfs based on the objects' spectral types. The other 7 (= 19 − 12) objects do not have K_{2MASS} data so we first convert their K_{MKO} (6 objects) or J_{MKO} (1 object) photometry into 2MASS photometry using their spectra and then apply the corresponding Filippazzo et al. (2015) bolometric correction for young objects. We also have 4 T8−T9 candidates with parallaxes, and these objects' spectral types exceed the applicable range (M7−T7) of the Filippazzo et al. (2015) bolometric corrections. Therefore, we use the super-magnitude method of Dupuy & Kraus (2013) as updated by W. Best et al. (in preparation). Briefly, this method computes bolometric luminosities for a set of absolute magnitudes composed of (1) J_{MKO}, H_{MKO}, *Spitzer*/IRAC [3.6], and *Spitzer*/IRAC [4.5] bands, (2) J_{MKO}, H_{MKO}, $W1$, $W2$ bands, or (3) subsets of the first two lists, using polynomials determined from the Sonora-Bobcat cloudless model atmospheres (Marley et al. 2017; Marley et al. in prep). Among these 4 objects, WISE J2255 − 3118 has IRTF/SpeX spectra and has been recently analyzed by us using Sonora-Bobcat models (Zhang et al. 2020c). Zhang et al. (2020c) also computed this object's L_{bol} by integrating its observed 1.0 − 2.5 μm SpeX spectrum and fitted model spectra to shorter and longer wavelengths spanning 0.4 − 50 μm. The resulting spectroscopic $L_{bol} = -5.72 \pm 0.03$ dex is consistent with our super-magnitude $L_{bol} = -5.79 \pm 0.06$ dex adopted in this work. Given that the Filippazzo et al. (2015) bolometric corrections were also based on integrating spectral energy distributions of objects, there does not seem to be signifi-

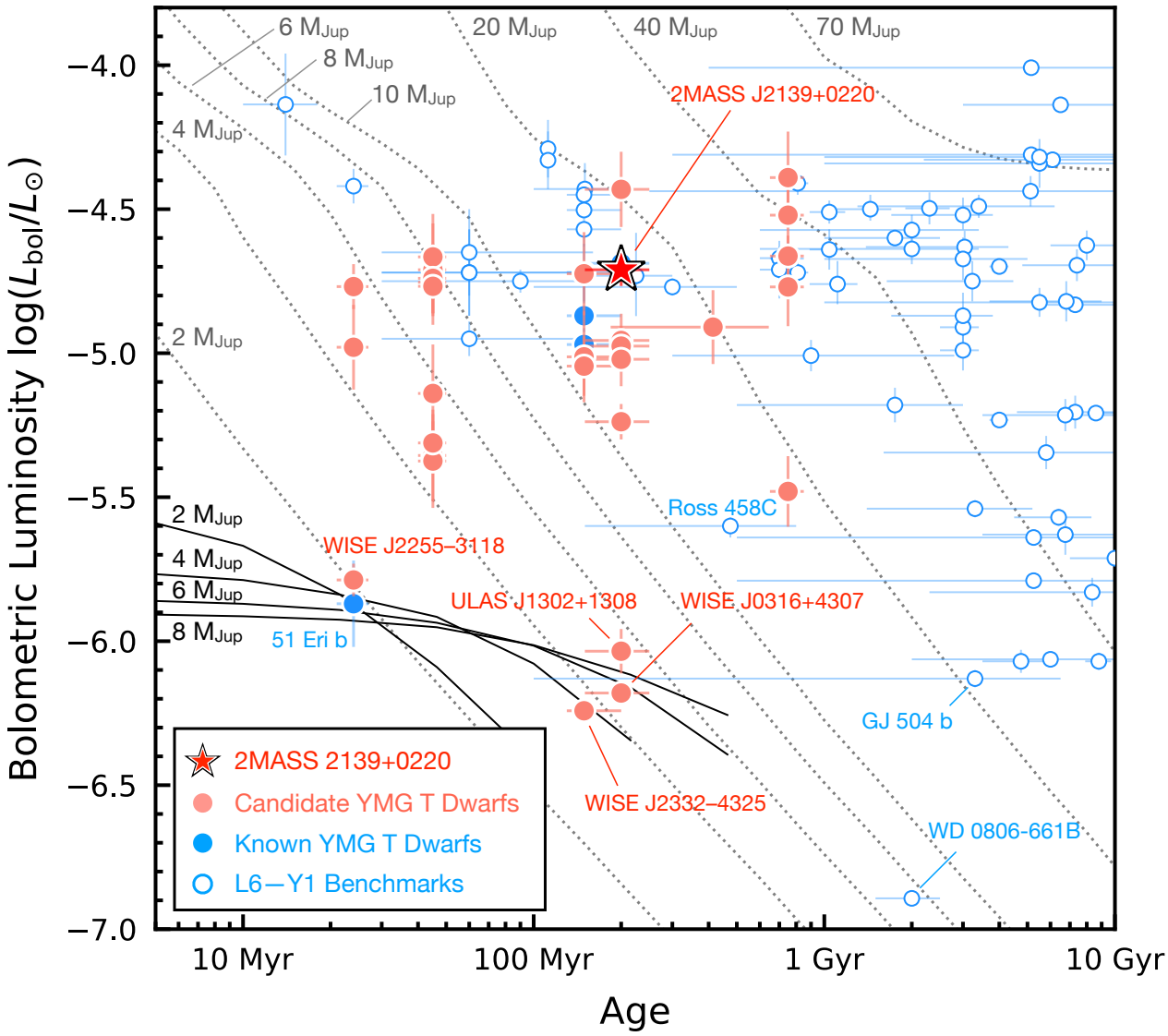

Figure 5. Derived bolometric luminosities and ages of our identified candidates (light red), by assuming they are all YMG members. We use the red star to mark our newly confirmed Carina-Near member 2MASS J2139 + 0220 and use blue solid circles for our recovered YMG T dwarfs. We overlay the L6−Y1 benchmarks (blue open circles) compiled by Zhang et al. (2020a) and this work (Tables 4 and 5), the hot-start Saumon & Marley (2008) hybrid evolutionary models (dashed grey lines), and the cold-start Fortney et al. (2008) evolutionary models (black solid lines). We find WISE J0316 + 4307 (T8), WISE J2255 − 3118 (T8), ULAS J1302 + 1308 (T8.5), and WISE J2332 − 4325 (T9) are all potential analogs of 51 Eri b, having much fainter $L_{\rm bol}$ than the other benchmark ultracool dwarfs with similar ages.

cant systematics in $L_{\rm bol}$ between our subsets of T0−T7 and T8−T9 candidates. For the remaining 7 (= 30 − 19 − 4) objects without trigonometric parallaxes, we use their photometric distances and convert their $K_{\rm MKO}$-band absolute magnitudes into $K_{\rm 2MASS}$ band using their spectra or polynomials provided by Filippazzo et al. (2015). Then, we apply the Filippazzo et al. (2015) bolometric correction for young ultracool dwarfs to compute these objects' bolometric luminosities. We have propagated all uncertainties in magnitudes, parallaxes, spectral types, and empirical relations into our resulting $L_{\rm bol}$ values in a Monte Carlo fashion.

We adopt YMG ages of 149^{+51}_{-19} Myr for AB Doradus (Bell et al. 2015), 40 − 50 Myr for Argus (Zuckerman 2019), 24 ± 3 Myr for β Pictoris (Bell et al. 2015), 200 ± 50 Myr for Carina-Near (Zuckerman et al. 2006), 750 ± 100 Myr for Hyades (Brandt & Huang 2015)[5], and 414 ± 23 Myr for the

[5] The Hyades open cluster mentioned here is the core of, and thereby distinct from, the Hyades supercluster (a.k.a. Hyades stream or Hyades moving

Ursa Major cluster (Jones et al. 2015). Combining our candidates' L_{bol} and ages, we then interpolate the hot-start Saumon & Marley (2008) hybrid evolutionary models and compute their effective temperatures (T_{eff}), surface gravities ($\log g$), radii (R), and masses (M) in a Monte Carlo fashion. We assume the objects' bolometric luminosities follow a normal distribution and assume their ages follow a uniform distribution (for Argus members) or a Gaussian distribution (for all other YMGs) constrained to $0-10$ Gyr. The derived physical properties of our 30 candidates are listed in Table 3 and shown in Figure 5. In total, 22 objects have planetary masses ($2-13$ M_{Jup}) if their memberships are confirmed.

We compare bolometric luminosities and ages of our candidates with all previously known L6−Y1 ultracool dwarfs with independently determined ages or masses (75 total benchmarks), including YMG members, wide-orbit companions to stars or white dwarfs, and ultracool binary systems with measured dynamical masses. We obtain properties of L6−T6 benchmarks (60 objects) from Zhang et al. (2020a), and we compile a catalog for T7−Y1 benchmarks (15 objects) in this work (Tables 4 and 5). We obtain L_{bol} of 11 T7−Y1 benchmarks from the literature, computed by integrating the objects' spectral energy distributions. Bolometric luminosities of the remaining 4 objects are either lacking (WISEU J005559.88+594745.0, Wolf 1130C, WD 0806−661B) or from a model-based bolometric correction in $W2$ band (WISE J111838.70+312537.9; see Wright et al. 2013), and therefore we (re-)compute their L_{bol} using the aforementioned super-magnitude method.

Among these 15 T7−Y1 benchmarks, dynamical masses have been measured for Gl 229B (Brandt et al. 2020) and Gl 758B (Bowler et al. 2018; Brandt et al. 2019). Following the rejection sampling analysis in Dupuy & Liu (2017), Brandt et al. (2020) combined the dynamical mass and L_{bol} of Gl 229B to derive its age, T_{eff}, $\log g$, and R using the Saumon & Marley (2008) hybrid evolutionary models. In this work, we conduct the same analysis for Gl 758B by using the more recent dynamical mass measured by Brandt et al. (2019; also see Bowler et al. 2018; Calissendorff & Janson 2018). For the remaining 13 benchmarks with no independently inferred masses, we obtain their ages from their host stars as determined in the literature. We then derive these objects' T_{eff}, $\log g$, R, and M by using their L_{bol}, ages, and the interpolated Saumon & Marley (2008) hybrid evolutionary models as done for our YMG candidates. For the two benchmarks older than $\sim$ 10 Gyr, WISEU J005559.88+594745.0 (10 ± 3 Gyr; Meisner et al. 2020) and Wolf 1130C (> 10 Gyr; Mace et al. 2018), we derive their physical properties at an age of 10 Gyr.

As shown in Figure 5, we find our 4 latest-type candidates, WISE J0316+4307 (T8), WISE J2255−3118 (T8), ULAS J1302+1308 (T8.5), and WISE J233226.49−432510.6 (WISE J2332−4325; T9) have comparably low luminosities and young ages as 51 Eri b, with the bolometric luminosities being much fainter than other benchmark ultracool dwarfs with similar ages. We discuss these objects in the following section.

3.4. *Individual Notable Objects*

3.4.1. *2MASS J2139+0220: A Newly Confirmed Member of the Carina-Near Moving Group*

2MASS J2139+0220 (T1.5) is the only object among our candidates that has full six-dimensional kinematic data (proper motion, parallax, and radial velocity). It has a high membership probability (95.9%) in the Carina-Near moving group (200 ± 50 Myr) based on BANYAN Σ. Its membership probability is only 1% based on LACEwING, which is known to produce a very low recovery rate for Carina-Near (see Section 7.15 of Riedel et al. 2017). This object's $XYZUVW$ position lines up well with those of previously known Carina-Near members (Figure 6), with UVW space motion very close to a member of the Carina-Near stream (GJ 907.1; K8) as defined by Zuckerman et al. (2006).

Previous work has studied near-infrared spectra of 2MASS J2139+0220 and derived its physical properties including surface gravity as an age indicator. Radigan et al. (2012) fitted this object's IRTF/SpeX spectra (e.g., Figure 4) using the ultracool atmospheric models described in Cushing et al. (2008) and Stephens et al. (2009) and developed by Ackerman & Marley (2001), Marley et al. (2002), Saumon & Marley (2008), and they inferred $\log g = 4.5$ dex, which is the lowest $\log g$ value where the models are defined. Apai et al. (2013) compared this object's *HST*/WFC3 G141 grism spectra ($1.05-1.7$ μm, $R\sim130$) with the Burrows et al. (2006) and the Allard et al. (2011) BT-Settl atmospheric models, and inferred $\log g$ of 4.0 dex and 4.5 dex, respectively. While these spectroscopically inferred surface gravities might contain modeling systematics, they are all consistent with our $\log g = 4.42^{+0.12}_{-0.06}$ dex based on evolutionary models and the assumption of its YMG membership (Section 3.3). More recent work by Vos et al. (2017) inferred a much higher $\log g$ of 5.37 ± 0.02 dex based on the Keck/NIRSPEC spectra ($2.29-2.33$ μm, $R\sim25,000$), but such $\log g$ might be less reliable given the narrow wavelength coverage and the lack of gravity-sensitive lines in the data.

group) proposed by Olin Eggen (e.g., Eggen 1958). It was initially hypothesized that members of the Hyades supercluster are coeval, but in fact this supercluster is composed of both young and field-age stars with a range of elemental abundances (e.g., Chereul & Grenon 2001; Famaey et al. 2005, 2007; Bovy & Hogg 2010; de Silva et al. 2011). Throughout this work, we follow Gagné et al. (2018b) and use the Hyades designation to refer to the young open cluster (750 ± 100 Myr; Brandt & Huang 2015), with members compiled by Perryman et al. (1998).

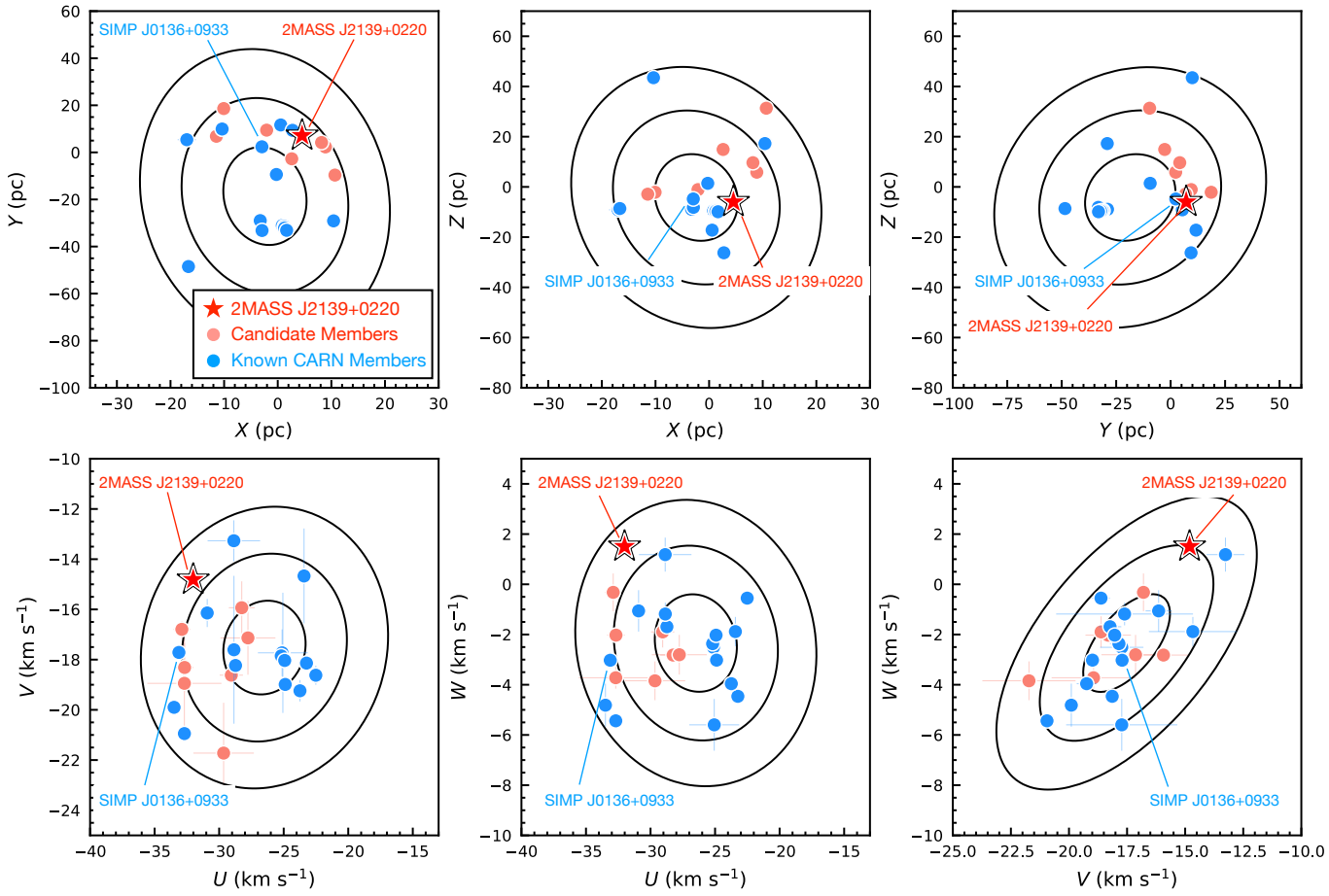

Figure 6. Galactic *XYZUVW* coordinates of our newly confirmed member 2MASS J2139 + 0220 (red star), our new candidate members (light red circles), and previously known members (blue circles) of the Carina-Near moving group (Zuckerman et al. 2006). We obtain kinematic information of previously known members from Gagné et al. (2018b) and use the BANYAN Σ multivariate Gaussian model to generate $1\sigma/2\sigma/3\sigma$ extent of this group's *XYZUVW* properties (black contours), with these contours encompassing 39.3% (1σ), 86.5% (2σ), and 98.9% (3σ) of the cumulative volume for each bivariate Gaussian distribution. For our candidate members with no radial velocity, we use light red circles to mark their optimal *UVW* space motions as Carina-Near members as computed by BANYAN Σ.

2MASS J2139 + 0220 is the most variable ultracool dwarf known to date (Radigan et al. 2012), and the coexistence of its very high variability and potential young age (thereby low $\log g$) is in accord with a tentative correlation between low surface gravity and high-amplitude variability of mid-L and L/T transition dwarfs (e.g., Metchev et al. 2015; Biller et al. 2015; Lew et al. 2016; Vos et al. 2018; Schneider et al. 2018; Bowler et al. 2020; Zhou et al. 2020). Photometric variability has been also detected in previously known T-dwarf YMG members. SIMP J013656.5+093347.3 (SIMP J0136 + 0933) is a T2.5 member of the same Carina-Near moving group identified by Gagné et al. (2017) and has a ≈ 5% variability in *J* band (Artigau et al. 2009; Radigan et al. 2014; Vos et al. 2017). GU Psc b (Naud et al. 2014) and 2MASS J1324 + 6358 (Gagné et al. 2018a) are both members of the AB Doradus moving group, with variability of ≈ 4% in *J* band (for GU Psc b detected by Naud et al. 2017a) or ≈ 3% in the mid-infrared (for 2MASS J1324 + 6358 detected by Metchev et al. 2015). The high-amplitude variability of 2MASS J2139 + 0220 is likely related to its peculiar spectrum (Figure 3) and might also have the impact on its redder, fainter near-infrared photometry compared to field dwarfs (Figure 2; e.g., Lew et al. 2020).

To summarize, we assign 2MASS J2139 + 0220 as a new kinematic member of the Carina-Near moving group, making it the second T dwarf (after SIMP J0136 + 0933 [T2.5]) in this group, as well as the third closest group member to Earth (after SIMP J0136 + 0933 [6.11 ± 0.03 pc] and GJ 358 [9.601 ± 0.004 pc]).

3.4.2. *Young Late-T Candidates: WISE J0316 + 4307, ULAS J1302 + 1308, WISE J2255 − 3118, and WISE J2332 − 4325*

As seen in Figure 5, our 4 latest-type candidates have much fainter $L_{\rm bol}$ than other ultracool benchmarks with simi-

lar ages. WISE J0316+4307 (T8) and ULAS J1302+1308 (T8.5) are both candidate members of the Carina-Near moving group (200 ± 50 Myr) with BANYAN Σ probabilities of 95.4% and 97.7%, resepctively. Their membership probabilities are both 0% based on LACEwING, which is known to produce a very low recovery rate for confirmed members of Carina-Near (see Section 7.15 of Riedel et al. 2017). WISE J0316+4307 has Keck/NIRSPEC spectra in J and H bands (Mace et al. 2013a) which show no anomalies when compared to NIRSPEC spectra (McLean et al. 2003) of the T8 spectral standard, 2MASSI J0415195−093506 (2MASS J0415−0935; Burgasser et al. 2006). However, WISE J0316+4307 has $\sim$2 mag fainter J- and H-band absolute magnitudes than typical field T8 dwarfs. ULAS J1302+1308 has much redder $J-K$ and $H-K$ colors than other T8−T9 field dwarfs (Figure 2), and its Subaru/IRCS spectrum has slightly enhanced fluxes near the Y-band peak as compared to 2MASS J0415−0935, likely suggesting a lower surface gravity based on the Sonora-Bobcat cloudless models (Marley et al. 2017; Marley et al. in prep; e.g., see Figure 1 of Zhang et al. 2020b).

WISE J2255−3118 (T8) is a candidate member of the β Pictoris moving group (24 ± 3 Myr) with a 98.7% BANYAN Σ probability and a 32% LACEwING probability. Similar to ULAS J1302+1308, WISE J2255−3118 also has unusually red $J-K$ and $H-K$ colors (Figure 2), with a slightly enhanced Y-band peak flux compared to the T8 spectral standard 2MASS J0415−0935, indicative of a lower surface gravity. Recently, we (Zhang et al. 2020c) have analyzed the IRTF/SpeX spectra of late-T dwarfs using the cloudless Sonora-Bobcat models, with WISE J2255−3118 included in our sample. Our spectroscopically inferred surface gravity $\log g = 3.66^{+0.32}_{-0.30}$ dex of WISE J2255−3118 is among the lowest in our entire late-T dwarf sample, and is also consistent with its $\log g = 3.54^{+0.03}_{-0.02}$ dex in this work using the evolutionary models with assumed YMG membership (Section 3.3 and Table 3).

WISE J2332−4325 (T9) is a candidate member of the AB Doradus moving group (149^{+51}_{-19} Myr) with a BANYAN Σ probability of 98.9%. This object has J-band Keck/NIRSPEC spectra (Tinney et al. 2018) consistent with the T9 spectral standard UGPS J072227.51−054031.2 (Cushing et al. 2011). However, WISE J2332−4325 has a much fainter J-band absolute magnitude and redder $J-H$ color than typical field T9 dwarfs (Figure 2).

The anomalous spectrophotometric appearance of these 4 objects is very similar to the β Pictoris moving group exoplanet 51 Eri b (T6.5; Macintosh et al. 2015), which also has unusually faint absolute magnitudes and red near-infrared colors. Moreover, all these objects have distinctly faint $L_{\rm bol}$ as compared to other ultracool benchmarks with similar ages (Figure 5). Radial velocity follow-up is needed to assess the YMG membership of these 4 candidates, and if their young ages are confirmed, they will become the latest-type kinematic members of any young moving groups or associations. Most notably, they will be the first free-floating planets, whose physical properties are compatible with formation by both hot-start (with high initial entropy and no subsequent accretion; e.g., Burrows et al. 1997; Chabrier 2001; Baraffe et al. 2003; Saumon & Marley 2008) and cold-start (with low initial entropy and core accretion; e.g., Marley et al. 2007; Fortney et al. 2008) conditions. These late-type YMG members may therefore shed insight on the formation pathways of directly-imaged and free-floating planets.

4. SUMMARY

We have identified new and candidate T-dwarf members of nearby young moving using astrometry for 694 T and Y dwarfs, including 447 objects with parallaxes, mostly produced by recent large near-infrared astrometric programs by Kirkpatrick et al. (2019) and Best et al. (2020a). Using the BANYAN Σ and LACEwING algorithms, we have recovered all 5 previously known T-dwarf YMG members and identified 30 new candidate members.

We find 4 early-T (including 2MASS J2139+0220) and 3 late-T candidate members exhibit $0.4-0.8$ mag redder $J-K$ colors and/or $0.6-2.2$ mag fainter J-band absolute magnitudes than field dwarfs with similar spectral types. Such anomalous photometry is in accord with previously known YMG T dwarfs (e.g., 2MASS J1324+6358 and 51 Eri b), providing evidence of their youth and thereby supporting YMG membership.

Several of our candidates show unusual spectral features that differ from single ultracool dwarfs. Such peculiarities are consistent with unresolved binarity. Alternatively, these objects might have inhomogeneous cloud cover and/or temperature fluctuations, which cause their spectra to appear like the sum of photospheres with different effective temperatures. Variability monitoring would help to investigate their spectral peculiarities.

We have estimated bolometric luminosities of all our candidates and inferred their effective temperatures, surface gravities, radii, and masses from evolutionary models assuming they are YMG members. The resulting mass estimates for 22 out of 30 candidates span $2-13$ $M_{\rm Jup}$, firmly in the planetary-mass regime. We establish the high-amplitude variable T1.5 dwarf 2MASS J2139+0220 as a new planetary-mass member ($14.6^{+3.2}_{-1.6}$ $M_{\rm Jup}$) of the Carina-Near (200 ± 50 Myr) moving group, making it the second T dwarf and the third closest member of this group. 2MASS J2139+0220 is the most variable ultracool dwarf found to date, and the coexistence of its variability and youth is in accord with a tentative correlation between low surface gravity and high-amplitude variability of mid-L and L/T

transition objects. Its high variability might also be related to its unusually red, faint near-infrared photometry and peculiar spectrum.

Our four latest-type YMG candidates have spectral types of T8−T9. If confirmed, these objects will be the first free-floating planets whose ages and luminosities are compatible with both hot-start and cold-start evolutionary models, and thereby overlap the planetary-mass companion 51 Eri b. The low surface gravity of these objects are also supported by their anomalous spectrophotometry and our recent atmospheric modeling for one of them (WISE J2255 − 3118). Along with this analysis, we have also compiled all 15 previously known L7−Y1 benchmarks and derived a homogeneous set of their effective temperatures, surface gravities, radii, and masses.

Radial velocity measurements are needed to assess the membership of our YMG candidates except for 2MASS J2139+0220. Such follow-up is feasible for our brightest candidates using existing high-resolution spectrographs on 8−10 meter-class telescopes (e.g., Gemini/GNIRS and Keck/NIRSPEC), but the majority of our candidates are too faint ($J \gtrsim 16.5$ mag, $K \gtrsim 15$ mag) and await 20−30 meter-class telescopes for radial velocity characterization.

This work has benefited from The UltracoolSheet at http://bit.ly/UltracoolSheet, maintained by Will Best, Trent Dupuy, Michael Liu, Rob Siverd, and Zhoujian Zhang, and developed from compilations by Dupuy & Liu (2012), Dupuy & Kraus (2013), Liu et al. (2016), Best et al. (2018), and Best et al. (2021). M.C.L. acknowledges National Science Foundation (NSF) grant AST-1518339. This research was greatly facilitated by the TOPCAT software written by Mark Taylor (http://www.starlink.ac.uk/topcat/). Finally, the authors wish to recognize and acknowledge the very significant cultural role and reverence that the summit of Maunakea has always had within the indigenous Hawaiian community. We are most fortunate to have the opportunity to conduct observations from this mountain.

Facilities: IRTF (SpeX), CFHT (WIRCam)

Software: BANYAN Σ (version 1.2; Gagné et al. 2018b), LACEwING (Riedel et al. 2017), TOPCAT (Taylor 2005), Astropy (Astropy Collaboration et al. 2013, 2018), IPython (Pérez & Granger 2007), Numpy (Oliphant 2006), Scipy (Jones et al. 2001), Matplotlib (Hunter 2007).

REFERENCES

Ackerman, A. S., & Marley, M. S. 2001, ApJ, 556, 872, doi: 10.1086/321540

Albert, L., Artigau, É., Delorme, P., et al. 2011, AJ, 141, 203, doi: 10.1088/0004-6256/141/6/203

Allard, F., Homeier, D., & Freytag, B. 2011, Astronomical Society of the Pacific Conference Series, Vol. 448, Model Atmospheres From Very Low Mass Stars to Brown Dwarfs, ed. C. Johns-Krull, M. K. Browning, & A. A. West, 91

Apai, D., Radigan, J., Buenzli, E., et al. 2013, ApJ, 768, 121, doi: 10.1088/0004-637X/768/2/121

Artigau, É., Bouchard, S., Doyon, R., & Lafrenière, D. 2009, ApJ, 701, 1534, doi: 10.1088/0004-637X/701/2/1534

Artigau, É., Doyon, R., Lafrenière, D., et al. 2006, ApJL, 651, L57, doi: 10.1086/509146

Astropy Collaboration, Robitaille, T. P., Tollerud, E. J., et al. 2013, A&A, 558, A33, doi: 10.1051/0004-6361/201322068

Astropy Collaboration, Price-Whelan, A. M., Sipőcz, B. M., et al. 2018, AJ, 156, 123, doi: 10.3847/1538-3881/aabc4f

Baraffe, I., Chabrier, G., Barman, T. S., Allard, F., & Hauschildt, P. H. 2003, A&A, 402, 701, doi: 10.1051/0004-6361:20030252

Bardalez Gagliuffi, D. C., Gelino, C. R., & Burgasser, A. J. 2015, AJ, 150, 163, doi: 10.1088/0004-6256/150/5/163

Bardalez Gagliuffi, D. C., Burgasser, A. J., Gelino, C. R., et al. 2014, ApJ, 794, 143, doi: 10.1088/0004-637X/794/2/143

Barman, T. S., Macintosh, B., Konopacky, Q. M., & Marois, C. 2011, ApJ, 733, 65, doi: 10.1088/0004-637X/733/1/65

Bell, C. P. M., Mamajek, E. E., & Naylor, T. 2015, MNRAS, 454, 593, doi: 10.1093/mnras/stv1981

Best, W. M. J., Dupuy, T. J., Liu, M. C., Siverd, R. J., & Zhang, Z. 2020b, The UltracoolSheet: Photometry, Astrometry, Spectroscopy, and Multiplicity for 3000+ Ultracool Dwarfs and Imaged Exoplanets, Zenodo, doi: 10.5281/zenodo.4169085

Best, W. M. J., Liu, M. C., Magnier, E. A., & Dupuy, T. J. 2020a, AJ, 159, 257, doi: 10.3847/1538-3881/ab84f4

—. 2021, AJ, 161, 42, doi: 10.3847/1538-3881/abc893

Best, W. M. J., Liu, M. C., Magnier, E. A., et al. 2013, ApJ, 777, 84, doi: 10.1088/0004-637X/777/2/84

—. 2015, ApJ, 814, 118, doi: 10.1088/0004-637X/814/2/118

—. 2017, ApJ, 837, 95, doi: 10.3847/1538-4357/aa5df0

Best, W. M. J., Magnier, E. A., Liu, M. C., et al. 2018, ApJS, 234, 1, doi: 10.3847/1538-4365/aa9982

Biller, B. A., Vos, J., Bonavita, M., et al. 2015, ApJL, 813, L23, doi: 10.1088/2041-8205/813/2/L23

Bouvier, J., Kendall, T., Meeus, G., et al. 2008, A&A, 481, 661, doi: 10.1051/0004-6361:20079303

Bovy, J., & Hogg, D. W. 2010, ApJ, 717, 617, doi: 10.1088/0004-637X/717/2/617

Bowler, B. P., Zhou, Y., Morley, C. V., et al. 2020, ApJL, 893, L30, doi: 10.3847/2041-8213/ab8197

Bowler, B. P., Liu, M. C., Mawet, D., et al. 2017, AJ, 153, 18, doi: 10.3847/1538-3881/153/1/18

Bowler, B. P., Dupuy, T. J., Endl, M., et al. 2018, AJ, 155, 159, doi: 10.3847/1538-3881/aab2a6

Bowler, B. P., Hinkley, S., Ziegler, C., et al. 2019, ApJ, 877, 60, doi: 10.3847/1538-4357/ab1018

Brandt, T. D., Dupuy, T. J., & Bowler, B. P. 2019, AJ, 158, 140, doi: 10.3847/1538-3881/ab04a8

Brandt, T. D., Dupuy, T. J., Bowler, B. P., et al. 2020, AJ, 160, 196, doi: 10.3847/1538-3881/abb45e

Brandt, T. D., & Huang, C. X. 2015, ApJ, 807, 24, doi: 10.1088/0004-637X/807/1/24

Burgasser, A. J. 2014, in Astronomical Society of India Conference Series, Vol. 11, Astronomical Society of India Conference Series, 7–16

Burgasser, A. J., Cruz, K. L., Cushing, M., et al. 2010a, ApJ, 710, 1142, doi: 10.1088/0004-637X/710/2/1142

Burgasser, A. J., Geballe, T. R., Leggett, S. K., Kirkpatrick, J. D., & Golimowski, D. A. 2006, ApJ, 637, 1067, doi: 10.1086/498563

Burgasser, A. J., Looper, D., & Rayner, J. T. 2010b, AJ, 139, 2448, doi: 10.1088/0004-6256/139/6/2448

Burgasser, A. J., Kirkpatrick, J. D., Cutri, R. M., et al. 2000, ApJL, 531, L57, doi: 10.1086/312522

Burgasser, A. J., Simcoe, R. A., Bochanski, J. J., et al. 2010c, ApJ, 725, 1405, doi: 10.1088/0004-637X/725/2/1405

Burningham, B., Pinfield, D. J., Leggett, S. K., et al. 2009, MNRAS, 395, 1237, doi: 10.1111/j.1365-2966.2009.14620.x

Burningham, B., Pinfield, D. J., Lucas, P. W., et al. 2010a, MNRAS, 406, 1885, doi: 10.1111/j.1365-2966.2010.16800.x

Burningham, B., Leggett, S. K., Lucas, P. W., et al. 2010b, MNRAS, 404, 1952, doi: 10.1111/j.1365-2966.2010.16411.x

Burningham, B., Cardoso, C. V., Smith, L., et al. 2013, MNRAS, 433, 457, doi: 10.1093/mnras/stt740

Burrows, A., Hubbard, W. B., Lunine, J. I., & Liebert, J. 2001, Reviews of Modern Physics, 73, 719, doi: 10.1103/RevModPhys.73.719

Burrows, A., Sudarsky, D., & Hubeny, I. 2006, ApJ, 640, 1063, doi: 10.1086/500293

Burrows, A., Marley, M., Hubbard, W. B., et al. 1997, ApJ, 491, 856, doi: 10.1086/305002

Calissendorff, P., & Janson, M. 2018, A&A, 615, A149, doi: 10.1051/0004-6361/201833309
Chabrier, G. 2001, ApJ, 554, 1274, doi: 10.1086/321401
Chambers, K. C., Magnier, E. A., Metcalfe, N., et al. 2016, arXiv e-prints. https://arxiv.org/abs/1612.05560
Chereul, E., & Grenon, M. 2001, in Astronomical Society of the Pacific Conference Series, Vol. 228, Dynamics of Star Clusters and the Milky Way, ed. S. Deiters, B. Fuchs, A. Just, R. Spurzem, & R. Wielen, 398
Chiu, K., Fan, X., Leggett, S. K., et al. 2006, AJ, 131, 2722, doi: 10.1086/501431
Crundall, T. D., Ireland, M. J., Krumholz, M. R., et al. 2019, MNRAS, 489, 3625, doi: 10.1093/mnras/stz2376
Cushing, M. C., Marley, M. S., Saumon, D., et al. 2008, ApJ, 678, 1372, doi: 10.1086/526489
Cushing, M. C., Kirkpatrick, J. D., Gelino, C. R., et al. 2011, ApJ, 743, 50, doi: 10.1088/0004-637X/743/1/50
Cutri, R. M., Skrutskie, M. F., van Dyk, S., et al. 2003, 2MASS All Sky Catalog of point sources.
Cutri, R. M. e. 2014, VizieR Online Data Catalog, 2328
Dahn, C. C., Harris, H. C., Subasavage, J. P., et al. 2017, AJ, 154, 147, doi: 10.3847/1538-3881/aa880b
Day-Jones, A. C., Marocco, F., Pinfield, D. J., et al. 2013, MNRAS, 430, 1171, doi: 10.1093/mnras/sts685
de Silva, G. M., Freeman, K. C., Bland-Hawthorn, J., et al. 2011, MNRAS, 415, 563, doi: 10.1111/j.1365-2966.2011.18728.x
Dupuy, T. J., & Kraus, A. L. 2013, Science, 341, 1492, doi: 10.1126/science.1241917
Dupuy, T. J., & Liu, M. C. 2012, ApJS, 201, 19, doi: 10.1088/0067-0049/201/2/19
—. 2017, ApJS, 231, 15, doi: 10.3847/1538-4365/aa5e4c
Dupuy, T. J., Liu, M. C., Leggett, S. K., et al. 2015, ApJ, 805, 56, doi: 10.1088/0004-637X/805/1/56
Dupuy, T. J., Liu, M. C., Allers, K. N., et al. 2018, AJ, 156, 57, doi: 10.3847/1538-3881/aacbc2
Edge, A., Sutherland, W., & Viking Team. 2016, VizieR Online Data Catalog, II/343
Eggen, O. J. 1958, MNRAS, 118, 65, doi: 10.1093/mnras/118.1.65
Eisenhardt, P. R. M., Marocco, F., Fowler, J. W., et al. 2020, ApJS, 247, 69, doi: 10.3847/1538-4365/ab7f2a
Eriksson, S. C., Janson, M., & Calissendorff, P. 2019a, A&A, 629, A145, doi: 10.1051/0004-6361/201935671
—. 2019b, A&A, 629, A145, doi: 10.1051/0004-6361/201935671
Faherty, J. K., Riedel, A. R., Cruz, K. L., et al. 2016, ApJS, 225, 10, doi: 10.3847/0067-0049/225/1/10
Faherty, J. K., Goodman, S., Caselden, D., et al. 2020, ApJ, 889, 176, doi: 10.3847/1538-4357/ab5303
Famaey, B., Jorissen, A., Luri, X., et al. 2005, A&A, 430, 165, doi: 10.1051/0004-6361:20041272
Famaey, B., Pont, F., Luri, X., et al. 2007, A&A, 461, 957, doi: 10.1051/0004-6361:20065706
Filippazzo, J. C., Rice, E. L., Faherty, J., et al. 2015, ApJ, 810, 158, doi: 10.1088/0004-637X/810/2/158
Fortney, J. J., Marley, M. S., Saumon, D., & Lodders, K. 2008, ApJ, 683, 1104, doi: 10.1086/589942
Gagné, J., Allers, K. N., Theissen, C. A., et al. 2018a, ApJL, 854, L27, doi: 10.3847/2041-8213/aaacfd
Gagné, J., Burgasser, A. J., Faherty, J. K., et al. 2015, ApJL, 808, L20, doi: 10.1088/2041-8205/808/1/L20
Gagné, J., & Faherty, J. K. 2018, ApJ, 862, 138, doi: 10.3847/1538-4357/aaca2e
Gagné, J., Faherty, J. K., Burgasser, A. J., et al. 2017, ApJL, 841, L1, doi: 10.3847/2041-8213/aa70e2
Gagné, J., Mamajek, E. E., Malo, L., et al. 2018b, ApJ, 856, 23, doi: 10.3847/1538-4357/aaae09
Gaia Collaboration, Prusti, T., de Bruijne, J. H. J., et al. 2016, A&A, 595, A1, doi: 10.1051/0004-6361/201629272
Gaia Collaboration, Brown, A. G. A., Vallenari, A., et al. 2018, A&A, 616, A1, doi: 10.1051/0004-6361/201833051
Goldman, B., Marsat, S., Henning, T., Clemens, C., & Greiner, J. 2010, MNRAS, 405, 1140, doi: 10.1111/j.1365-2966.2010.16524.x
Heintz, W. D. 1967, Astronomische Nachrichten, 289, 269, doi: 10.1002/asna.19662890603
Heinze, A. N., Metchev, S., & Kellogg, K. 2015, ApJ, 801, 104, doi: 10.1088/0004-637X/801/2/104
Herschel, W. 1804, Philosophical Transactions of the Royal Society of London Series I, 94, 353
Hewett, P. C., Warren, S. J., Leggett, S. K., & Hodgkin, S. T. 2006, MNRAS, 367, 454, doi: 10.1111/j.1365-2966.2005.09969.x
Hunter, J. D. 2007, Computing in Science & Engineering, 9, 90, doi: 10.1109/MCSE.2007.55
Janson, M., Carson, J., Thalmann, C., et al. 2011, ApJ, 728, 85, doi: 10.1088/0004-637X/728/2/85
Janson, M., Brandt, T. D., Kuzuhara, M., et al. 2013, ApJL, 778, L4, doi: 10.1088/2041-8205/778/1/L4
Jones, E., Oliphant, T., Peterson, P., et al. 2001, SciPy: Open source scientific tools for Python. http://www.scipy.org/
Jones, J., White, R. J., Boyajian, T., et al. 2015, ApJ, 813, 58, doi: 10.1088/0004-637X/813/1/58
Kellogg, K., Metchev, S., Miles-Páez, P. A., & Tannock, M. E. 2017, AJ, 154, 112, doi: 10.3847/1538-3881/aa83b0
Khandrika, H., Burgasser, A. J., Melis, C., et al. 2013, AJ, 145, 71, doi: 10.1088/0004-6256/145/3/71

Kharchenko, N. V., Scholz, R. D., Piskunov, A. E., Röser, S., & Schilbach, E. 2007, Astronomische Nachrichten, 328, 889, doi: 10.1002/asna.200710776

Kirkpatrick, J. D., Looper, D. L., Burgasser, A. J., et al. 2010, ApJS, 190, 100, doi: 10.1088/0067-0049/190/1/100

Kirkpatrick, J. D., Cushing, M. C., Gelino, C. R., et al. 2011, ApJS, 197, 19, doi: 10.1088/0067-0049/197/2/19

Kirkpatrick, J. D., Gelino, C. R., Cushing, M. C., et al. 2012, ApJ, 753, 156, doi: 10.1088/0004-637X/753/2/156

Kirkpatrick, J. D., Martin, E. C., Smart, R. L., et al. 2019, ApJS, 240, 19, doi: 10.3847/1538-4365/aaf6af

Kirkpatrick, J. D., Gelino, C. R., Faherty, J. K., et al. 2020, arXiv e-prints, arXiv:2011.11616. https://arxiv.org/abs/2011.11616

Knapp, G. R., Leggett, S. K., Fan, X., et al. 2004, AJ, 127, 3553, doi: 10.1086/420707

Kuzuhara, M., Tamura, M., Kudo, T., et al. 2013, ApJ, 774, 11, doi: 10.1088/0004-637X/774/1/11

Lawrence, A., Warren, S. J., Almaini, O., et al. 2007, MNRAS, 379, 1599, doi: 10.1111/j.1365-2966.2007.12040.x

—. 2012, VizieR Online Data Catalog, II/314

Leggett, S. K., Hauschildt, P. H., Allard, F., Geballe, T. R., & Baron, E. 2002, MNRAS, 332, 78, doi: 10.1046/j.1365-8711.2002.05273.x

Leggett, S. K., Morley, C. V., Marley, M. S., & Saumon, D. 2015, ApJ, 799, 37, doi: 10.1088/0004-637X/799/1/37

Leggett, S. K., Tremblin, P., Esplin, T. L., Luhman, K. L., & Morley, C. V. 2017, ApJ, 842, 118, doi: 10.3847/1538-4357/aa6fb5

Leggett, S. K., Burningham, B., Saumon, D., et al. 2010, ApJ, 710, 1627, doi: 10.1088/0004-637X/710/2/1627

Lew, B. W. P., Apai, D., Zhou, Y., et al. 2016, ApJL, 829, L32, doi: 10.3847/2041-8205/829/2/L32

—. 2020, AJ, 159, 125, doi: 10.3847/1538-3881/ab5f59

Liu, M. C., Dupuy, T. J., & Allers, K. N. 2016, ApJ, 833, 96, doi: 10.3847/1538-4357/833/1/96

Liu, M. C., Leggett, S. K., & Chiu, K. 2007, ApJ, 660, 1507, doi: 10.1086/512662

Liu, M. C., Magnier, E. A., Deacon, N. R., et al. 2013, ApJL, 777, L20, doi: 10.1088/2041-8205/777/2/L20

Luhman, K. L., Burgasser, A. J., & Bochanski, J. J. 2011, ApJL, 730, L9, doi: 10.1088/2041-8205/730/1/L9

Luhman, K. L., Burgasser, A. J., Labbé, I., et al. 2012, ApJ, 744, 135, doi: 10.1088/0004-637X/744/2/135

Luhman, K. L., Patten, B. M., Marengo, M., et al. 2007, ApJ, 654, 570, doi: 10.1086/509073

Mace, G. N., Kirkpatrick, J. D., Cushing, M. C., et al. 2013a, ApJS, 205, 6, doi: 10.1088/0067-0049/205/1/6

—. 2013b, ApJ, 777, 36, doi: 10.1088/0004-637X/777/1/36

Mace, G. N., Mann, A. W., Skiff, B. A., et al. 2018, ApJ, 854, 145, doi: 10.3847/1538-4357/aaa8dd

Macintosh, B., Graham, J. R., Barman, T., et al. 2015, Science, 350, 64, doi: 10.1126/science.aac5891

Magnier, E. A., Schlafly, E. F., Finkbeiner, D. P., et al. 2016, arXiv e-prints. https://arxiv.org/abs/1612.05242

Malo, L., Artigau, É., Doyon, R., et al. 2014, ApJ, 788, 81, doi: 10.1088/0004-637X/788/1/81

Malo, L., Doyon, R., Lafrenière, D., et al. 2013, ApJ, 762, 88, doi: 10.1088/0004-637X/762/2/88

Mamajek, E. E. 2005, ApJ, 634, 1385, doi: 10.1086/468181

Manjavacas, E., Goldman, B., Reffert, S., & Henning, T. 2013, A&A, 560, A52, doi: 10.1051/0004-6361/201321720

Manjavacas, E., Apai, D., Zhou, Y., et al. 2019, AJ, 157, 101, doi: 10.3847/1538-3881/aaf88f

Marley, M. S., Fortney, J. J., Hubickyj, O., Bodenheimer, P., & Lissauer, J. J. 2007, ApJ, 655, 541, doi: 10.1086/509759

Marley, M. S., Saumon, D., Fortney, J. J., et al. 2017, in American Astronomical Society Meeting Abstracts, Vol. 230, American Astronomical Society Meeting Abstracts #230, 315.07

Marley, M. S., Seager, S., Saumon, D., et al. 2002, ApJ, 568, 335, doi: 10.1086/338800

Marocco, F., Smart, R. L., Jones, H. R. A., et al. 2010, A&A, 524, A38, doi: 10.1051/0004-6361/201015394

Marocco, F., Jones, H. R. A., Day-Jones, A. C., et al. 2015, MNRAS, 449, 3651, doi: 10.1093/mnras/stv530

Marocco, F., Eisenhardt, P. R. M., Fowler, J. W., et al. 2020, arXiv e-prints, arXiv:2012.13084. https://arxiv.org/abs/2012.13084

McLean, I. S., McGovern, M. R., Burgasser, A. J., et al. 2003, ApJ, 596, 561, doi: 10.1086/377636

McMahon, R. G., Banerji, M., Gonzalez, E., et al. 2013, The Messenger, 154, 35

Meisner, A. M., Faherty, J. K., Kirkpatrick, J. D., et al. 2020, ApJ, 899, 123, doi: 10.3847/1538-4357/aba633

Metchev, S. A., & Hillenbrand, L. A. 2006, ApJ, 651, 1166, doi: 10.1086/507836

Metchev, S. A., Kirkpatrick, J. D., Berriman, G. B., & Looper, D. 2008, ApJ, 676, 1281, doi: 10.1086/524721

Metchev, S. A., Heinze, A., Apai, D., et al. 2015, ApJ, 799, 154, doi: 10.1088/0004-637X/799/2/154

Miles-Páez, P. A., Metchev, S., Luhman, K. L., Marengo, M., & Hulsebus, A. 2017, AJ, 154, 262, doi: 10.3847/1538-3881/aa9711

Mugrauer, M., Seifahrt, A., Neuhäuser, R., & Mazeh, T. 2006, MNRAS, 373, L31, doi: 10.1111/j.1745-3933.2006.00237.x

Nakajima, T., Oppenheimer, B. R., Kulkarni, S. R., et al. 1995, Nature, 378, 463, doi: 10.1038/378463a0

Naud, M.-E., Artigau, É., Doyon, R., et al. 2017a, AJ, 154, 129, doi: 10.3847/1538-3881/aa826b

Naud, M.-E., Artigau, É., Rowe, J. F., et al. 2017b, AJ, 154, 138, doi: 10.3847/1538-3881/aa83b7

Naud, M.-E., Artigau, É., Malo, L., et al. 2014, ApJ, 787, 5, doi: 10.1088/0004-637X/787/1/5

Nilsson, R., Veicht, A., Giorla Godfrey, P. A., et al. 2017, ApJ, 838, 64, doi: 10.3847/1538-4357/aa643c

Oliphant, T. 2006, NumPy: A guide to NumPy, USA: Trelgol Publishing. http://www.numpy.org/

Pérez, F., & Granger, B. E. 2007, Computing in Science and Engineering, 9, 21, doi: 10.1109/MCSE.2007.53

Perryman, M. A. C., Brown, A. G. A., Lebreton, Y., et al. 1998, A&A, 331, 81. https://arxiv.org/abs/astro-ph/9707253

Pinfield, D. J., Jones, H. R. A., Lucas, P. W., et al. 2006, MNRAS, 368, 1281, doi: 10.1111/j.1365-2966.2006.10213.x

Pinfield, D. J., Burningham, B., Tamura, M., et al. 2008, MNRAS, 390, 304, doi: 10.1111/j.1365-2966.2008.13729.x

Pinfield, D. J., Burningham, B., Lodieu, N., et al. 2012, MNRAS, 422, 1922, doi: 10.1111/j.1365-2966.2012.20549.x

Puget, P., Stadler, E., Doyon, R., et al. 2004, in Society of Photo-Optical Instrumentation Engineers (SPIE) Conference Series, Vol. 5492, Ground-based Instrumentation for Astronomy, ed. A. F. M. Moorwood & M. Iye, 978–987

Radigan, J., Jayawardhana, R., Lafrenière, D., et al. 2012, ApJ, 750, 105, doi: 10.1088/0004-637X/750/2/105

Radigan, J., Lafrenière, D., Jayawardhana, R., & Artigau, E. 2014, ApJ, 793, 75, doi: 10.1088/0004-637X/793/2/75

Rajan, A., Rameau, J., De Rosa, R. J., et al. 2017, AJ, 154, 10, doi: 10.3847/1538-3881/aa74db

Rayner, J. T., Toomey, D. W., Onaka, P. M., et al. 2003, PASP, 115, 362, doi: 10.1086/367745

Riedel, A. R., Blunt, S. C., Lambrides, E. L., et al. 2017, AJ, 153, 95, doi: 10.3847/1538-3881/153/3/95

Robin, A. C., Reylé, C., Derrière, S., & Picaud, S. 2003, A&A, 409, 523, doi: 10.1051/0004-6361:20031117

Saumon, D., & Marley, M. S. 2008, ApJ, 689, 1327, doi: 10.1086/592734

Schneider, A. C., Hardegree-Ullman, K. K., Cushing, M. C., Kirkpatrick, J. D., & Shkolnik, E. L. 2018, AJ, 155, 238, doi: 10.3847/1538-3881/aabfc2

Schneider, A. C., Windsor, J., Cushing, M. C., Kirkpatrick, J. D., & Shkolnik, E. L. 2017, AJ, 153, 196, doi: 10.3847/1538-3881/aa6624

Scholz, R. D. 2010, A&A, 510, L8, doi: 10.1051/0004-6361/201014078

Shkolnik, E. L., Anglada-Escudé, G., Liu, M. C., et al. 2012, ApJ, 758, 56, doi: 10.1088/0004-637X/758/1/56

Skemer, A. J., Morley, C. V., Zimmerman, N. T., et al. 2016, ApJ, 817, 166, doi: 10.3847/0004-637X/817/2/166

Smart, R. L., Bucciarelli, B., Jones, H. R. A., et al. 2018, MNRAS, 481, 3548, doi: 10.1093/mnras/sty2520

Stephens, D. C., Leggett, S. K., Cushing, M. C., et al. 2009, ApJ, 702, 154, doi: 10.1088/0004-637X/702/1/154

Strauss, M. A., Fan, X., Gunn, J. E., et al. 1999, ApJL, 522, L61, doi: 10.1086/312218

Taylor, M. B. 2005, in Astronomical Society of the Pacific Conference Series, Vol. 347, Astronomical Data Analysis Software and Systems XIV, ed. P. Shopbell, M. Britton, & R. Ebert, 29

Thalmann, C., Carson, J., Janson, M., et al. 2009, ApJL, 707, L123, doi: 10.1088/0004-637X/707/2/L123

Tinney, C. G., Burgasser, A. J., & Kirkpatrick, J. D. 2003, AJ, 126, 975, doi: 10.1086/376481

Tinney, C. G., Faherty, J. K., Kirkpatrick, J. D., et al. 2014, ApJ, 796, 39, doi: 10.1088/0004-637X/796/1/39

Tinney, C. G., Kirkpatrick, J. D., Faherty, J. K., et al. 2018, ApJS, 236, 28, doi: 10.3847/1538-4365/aabad3

Torres, C. A. O., Quast, G. R., da Silva, L., et al. 2006, A&A, 460, 695, doi: 10.1051/0004-6361:20065602

Tremblin, P., Phillips, M. W., Emery, A., et al. 2020, A&A, 643, A23, doi: 10.1051/0004-6361/202038771

van Leeuwen, F. 2007, A&A, 474, 653, doi: 10.1051/0004-6361:20078357

Vos, J. M., Allers, K. N., & Biller, B. A. 2017, ApJ, 842, 78, doi: 10.3847/1538-4357/aa73cf

Vos, J. M., Allers, K. N., Biller, B. A., et al. 2018, MNRAS, 474, 1041, doi: 10.1093/mnras/stx2752

Wenger, M., Ochsenbein, F., Egret, D., et al. 2000, A&AS, 143, 9, doi: 10.1051/aas:2000332

Wright, E. L., Eisenhardt, P. R. M., Mainzer, A. K., et al. 2010, AJ, 140, 1868, doi: 10.1088/0004-6256/140/6/1868

Wright, E. L., Skrutskie, M. F., Kirkpatrick, J. D., et al. 2013, AJ, 145, 84, doi: 10.1088/0004-6256/145/3/84

Yang, H., Apai, D., Marley, M. S., et al. 2016, ApJ, 826, 8, doi: 10.3847/0004-637X/826/1/8

Zhang, Z., Liu, M. C., Marley, M. S., et al. 2020c, ApJ, submitted

Zhang, Z., Liu, M. C., Marley, M. S., Line, M. R., & Best, W. M. J. 2020b, arXiv e-prints, arXiv:2011.12294. https://arxiv.org/abs/2011.12294

Zhang, Z., Liu, M. C., Best, W. M. J., et al. 2018, ApJ, 858, 41, doi: 10.3847/1538-4357/aab269

Zhang, Z., Liu, M. C., Hermes, J. J., et al. 2020a, ApJ, 891, 171, doi: 10.3847/1538-4357/ab765c

Zhou, Y., Bowler, B. P., Morley, C. V., et al. 2020, AJ, 160, 77, doi: 10.3847/1538-3881/ab9e04

Zuckerman, B. 2019, ApJ, 870, 27, doi: 10.3847/1538-4357/aaee66

Zuckerman, B., Bessell, M. S., Song, I., & Kim, S. 2006, ApJL, 649, L115, doi: 10.1086/508060

Zuckerman, B., Song, I., & Bessell, M. S. 2004, ApJL, 613, L65, doi: 10.1086/425036

Zuckerman, B., Song, I., Bessell, M. S., & Webb, R. A. 2001, ApJL, 562, L87, doi: 10.1086/337968

Table 1. T-Dwarf Members and Candidates of Young Moving Groups

Object	SpT	R.A.[a] (hh:mm:ss.ss)	Dec.[a] (dd:mm:ss.ss)	$\mu_\alpha \cos\delta$ (mas yr^{-1})	μ_δ (mas yr^{-1})	Parallax[b] (mas)	RV[c] (km s^{-1})	Membership Probability		References					
								BANYAN Σ	LACEwING	SpT	Coord.	PM	Parallax	RV	Membership
AB Doradus															
• New Candidate Members (with trigonometric parallax)															
WISE J163645.56−074325.1	T4.5	16:36:45.65	−07:43:24.24	-39.4 ± 1.3	-152.4 ± 1.7	33.0 ± 5.0	$[-16.7 \pm 1.4]$	81.6%	7.0%	21	31	36	41	···	43
WISEPA J062720.07−111428.8	T6	06:27:20.09	−11:14:24.36	-13.2 ± 1.2	-337.8 ± 1.1	75.0 ± 4.0	$[+25.0 \pm 1.0]$	99.0%	30.0%	13	31	40	40	···	43
WISE J233226.49−432510.6[d]	T9	23:32:26.54	−43:25:10.92	249.7 ± 1.2	-249.9 ± 1.5	65.3 ± 2.6	$[+13.7 \pm 1.5]$	98.9%	8.0%	15	22	40	40	···	43
• New Candidate Members (with photometric parallax)															
ULAS J081918.58+210310.4	T6	08:19:18.62	21:03:12.60	-58.0 ± 11.0	-181.0 ± 11.0	$[33.2 \pm 3.2]$	$[+9.0 \pm 1.8]$	86.3%	12.0%	18	31	18	42	···	43
• Recovered Previously-Known Members															
2MASS J13243553+6358281[d]	T2.5	13:24:35.50	63:58:27.84	-368.0 ± 4.0	-63.7 ± 2.7	79.0 ± 9.0	-23.7 ± 0.4	99.8%	64.0%	10	31	36	38	38	38
GU Psc b	T3.5	01:12:35.04	17:03:55.44	96.64 ± 0.13	-100.70 ± 0.11	21.00 ± 0.07	-1.5 ± 0.5	99.1%	72.0%	24	37	29,37	29,37	23	24
SDSSp J111010.01+011613.1	T5.5	11:10:10.01	01:16:12.72	-217.1 ± 0.7	-280.9 ± 0.6	52.1 ± 1.2	$+7.5 \pm 3.8$	99.3%	46.0%	4	31	14	14	26	26
Argus															
• New Candidate Members (with trigonometric parallax)															
SDSS J152103.24+013142.7	T3	15:21:03.24	01:31:42.60	-176.0 ± 4.0	43.0 ± 4.0	43.0 ± 6.0	$[-18.6 \pm 1.3]$	82.3%	0.0%	28	31	41	41	···	43
2MASS J00132229−1143006	T4	00:13:22.32	−11:43:00.48	214.0 ± 3.0	-27.0 ± 3.0	40.0 ± 3.0	$[+0.4 \pm 1.3]$	96.8%	0.0%	33	31	41	41	···	43
SDSS J020742.48+000056.2	T4.5	02:07:42.84	00:00:55.80	159.0 ± 3.0	-14.0 ± 4.0	29.0 ± 4.0	$[+12.6 \pm 1.3]$	95.6%	0.0%	4	31	11	11	···	43
WISE J024124.73−365328.0[d]	T7	02:41:24.74	−36:53:27.97	242.0 ± 1.5	148.4 ± 1.4	52.4 ± 2.7	$[+11.8 \pm 1.5]$	87.7%	5.0%	39	22	40	40	···	43
• New Candidate Members (with photometric parallax)															
ULAS J004757.41+154641.4	T2	00:47:57.43	15:46:41.16	147.0 ± 28.0	-12.0 ± 28.0	$[27.0 \pm 2.9]$	$[+2.2 \pm 3.1]$	80.1%	0.0%	19	22	16	42	···	43
PSO J168.1800−27.2264	T2.5	11:12:43.25	−27:13:36.12	-120.0 ± 120.0	100.0 ± 40.0	$[26.3 \pm 2.8]$	$[+8.2 \pm 6.7]$	83.4%	0.0%	25	22	25	42	···	43
ULAS J154701.84+005320.3	T5.5	15:47:01.80	00:53:21.12	-76.0 ± 11.0	7.0 ± 10.0	$[23.3 \pm 2.7]$	$[-20.9 \pm 1.8]$	95.3%	0.0%	8	22	18	42	···	43
ULAS J120744.65+133902.7	T6	12:07:44.62	13:39:02.88	-155.0 ± 12.0	1.0 ± 12.0	$[25.0 \pm 2.5]$	$[+1.5 \pm 1.5]$	90.6%	0.0%	9	22	18	42	···	43
ULAS J075829.83+222526.7	T6.5	07:58:29.78	22:25:27.84	-105.0 ± 10.0	-57.0 ± 11.0	$[38.2 \pm 3.6]$	$[+22.4 \pm 1.4]$	92.7%	1.0%	18	22	18	42	···	43
β Pictoris															
• New Candidate Members (with trigonometric parallax)															
WISEPA J081958.05−033529.0	T4	08:19:58.18	−03:35:26.88	-198.7 ± 2.6	-166.5 ± 2.2	72.0 ± 3.0	$[+16.1 \pm 1.0]$	83.9%	1.0%	13	31	41	41	···	43
CFBDS J232304.41−015232.3	T6	23:23:04.39	−01:52:32.88	93.3 ± 1.5	-63.4 ± 1.6	30.2 ± 2.2	$[-1.9 \pm 0.9]$	89.1%	1.0%	12	31	41	41	···	43
WISEPC J225540.74−311841.8[d]	T8	22:55:40.75	−31:18:42.12	300.2 ± 1.5	-162.1 ± 2.2	71.0 ± 4.0	$[+1.6 \pm 0.9]$	98.7%	31.0%	13	22	40	40	···	43
• Recovered Previously-Known Members															
51 Eri b	T6.5	04:37:36.14	−02:28:24.60	44.3 ± 0.2	-63.8 ± 0.2	33.58 ± 0.14	$+21.0 \pm 1.8$	99.9%	50.0%	34	29,37	29,37	29,37	6	1,27
Carina-Near															
• Newly Confirmed Member															
2MASS J21392676+0220226	T1.5	21:39:27.10	02:20:24.00	489.7 ± 0.7	125.0 ± 0.8	96.5 ± 1.1	-25.1 ± 0.3	95.9%	1.0%	4	22	43	43	35	43

Table 1 continued

Table 1 *(continued)*

Object	SpT	R.A.[a] (hh:mm:ss.ss)	Dec.[a] (dd:mm:ss.ss)	$\mu_\alpha \cos\delta$ (mas yr^{-1})	μ_δ (mas yr^{-1})	Parallax[b] (mas)	RV[c] (km s^{-1})	Membership Probability BANYAN Σ	Membership Probability LACEwING	References SpT	References Coord.	References PM	References Parallax	References RV	References Membership
• New Candidate Members (with trigonometric parallax)															
ULAS J131610.13+031205.5	T3	13:16:10.22	03:12:05.76	-221.6 ± 2.9	-20.0 ± 3.0	29.0 ± 2.4	$[-6.6 \pm 0.8]$	91.7%	0.0%	28	31	41	41	···	43
PSO J004.6359+56.8370	T4.5	00:18:32.57	56:50:12.84	376.0 ± 3.0	10.4 ± 2.7	47.0 ± 4.0	$[-0.7 \pm 1.0]$	90.8%	0.0%	41	31	41	41	···	43
WISE J223617.59+510551.9[d]	T5	22:36:16.80	51:05:48.12	708.6 ± 2.1	326.7 ± 2.5	102.8 ± 1.9	$[-10.6 \pm 1.0]$	98.0%	0.0%	17	31	41	41	···	43
SDSSp J162414.37+002915.6	T6	16:24:14.33	00:29:15.72	-372.9 ± 1.6	-9.1 ± 2.0	91.8 ± 1.2	$[-28.7 \pm 1.1]$	99.0%	0.0%	4	31	2	2,40	···	43
2MASSI J1553022+153236	T7	15:53:02.21	15:32:36.96	-385.9 ± 0.7	166.2 ± 0.9	75.1 ± 0.9	$[-25.7 \pm 1.0]$	89.6%	0.0%	4	31	14	14	···	43
WISE J031624.35+430709.1[d]	T8	03:16:24.41	43:07:08.76	372.4 ± 1.5	-225.9 ± 1.5	73.3 ± 2.8	$[+16.3 \pm 1.0]$	95.4%	0.0%	21	22	40	40	···	43
ULAS J130217.21+130851.2	T8.5	13:02:17.09	13:08:51.00	-445.0 ± 6.0	5.0 ± 7.0	65.0 ± 5.0	$[-4.4 \pm 0.8]$	97.7%	0.0%	9	22	20	20	···	43
• Recovered Previously-Known Members															
SIMP J013656.5+093347.3	T2.5	01:36:56.57	09:33:47.16	1239.0 ± 1.2	-17.4 ± 0.8	163.7 ± 0.7	$+11.5 \pm 0.4$	95.6%	0.0%	3	29,37	29,37	29,37	32	32
Hyades															
• New Candidate Members (with trigonometric parallax)															
PSO J069.7303+04.3834	T2	04:38:55.18	04:23:00.24	132.0 ± 4.0	10.0 ± 3.0	37.0 ± 6.0	$[+39.4 \pm 1.8]$	84.7%	78.0%	41	31	41	41	···	43
PSO J049.1159+26.8409	T2.5	03:16:27.60	26:50:27.96	201.1 ± 2.4	-52.8 ± 1.9	34.0 ± 3.0	$[+29.5 \pm 1.8]$	80.3%	45.0%	25	31	41	41	···	43
PSO J052.2746+13.3754	T3.5	03:29:05.66	13:22:31.80	273.0 ± 2.0	-20.7 ± 2.0	44.0 ± 3.0	$[+32.5 \pm 1.8]$	92.8%	63.0%	41	31	41	41	···	43
• New Candidate Members (with photometric parallax)															
WISEPA J030724.57+290447.6	T6.5	03:07:24.60	29:04:47.64	100.0 ± 300.0	-100.0 ± 300.0	$[38.5 \pm 3.7]$	$[+27.3 \pm 0.2]$	39.3%	82.0%[e]	13	22	13	42	···	43
• Recovered Previously-Known Candidate Members															
CFHT−Hy−20	T2.5	04:30:38.71	13:09:56.88	142.6 ± 1.6	-16.5 ± 1.7	30.8 ± 1.5	$[+40.4 \pm 2.0]$	98.7%	99.0%	30	31	30	30	···	7
Ursa Major															
• New Candidate Members (with trigonometric parallax)															
SDSS J125011.65+392553.9	T4	12:50:11.71	39:25:55.55	-42.0 ± 3.0	-830.5 ± 2.6	43.0 ± 3.0	$[-10.1 \pm 2.2]$	0.0%	78.0%	5	31	41	41	···	43

[a] Coordinates are provided at epoch J2000 with equinox J2000.

[b] Parallaxes inside brackets are derived from photometric distances.

[c] Radial velocities inside brackets are optimal values with the assumed YMG membership as inferred by BANYAN Σ (all candidates with membership probabilities $> 80\%$) or LACEwING (only for WISEPA J030724.57 + 290447.6 and SDSS J125011.65 + 392553.9).

[d] These six objects (5 YMG candidates and 1 previously known YMG member) also have parallaxes and proper motions from Kirkpatrick et al. (2020), which became available while our paper was under review. The new astrometry does not alter the candidacy of these objects, but does slightly change their BANYAN Σ membership probabilities to 99.4% (AB Doradus) for 2MASS J13243553+6358281, 95.5% (Argus) for WISE J024124.73−365328.0, 94.4% (Carina-Near) for WISE J031624.35+430709.1, 90.5% (Carina-Near) for WISE J223617.59+510551.9, 99.7% (AB Doradus) for WISE J233226.49−432510.6, and 99.1% (β Pictoris) for WISEPC J225540.74−311841.8. Also, 3 objects have their LACEwING membership probabilities changed to 55% (AB Doradus) for WISE J233226.49−432510.6, 62% (AB Doradus) for 2MASS J13243553+6358281, and 31% (β Pictoris) for WISEPC J225540.74−311841.8.

[e] Based on LACEwING, this object is also likely a member of the AB Doradus moving group with a probability of 40%.

References—(1) Zuckerman et al. (2001), (2) Tinney et al. (2003), (3) Artigau et al. (2006), (4) Burgasser et al. (2006), (5) Chiu et al. (2006), (6) Kharchenko et al. (2007), (7) Bouvier et al. (2008), (8) Pinfield et al. (2008), (9) Burningham et al. (2010a), (10) Kirkpatrick et al. (2010), (11) Marocco et al. (2010), (12) Albert et al. (2011), (13) Kirkpatrick et al. (2011), (14) Dupuy & Liu (2012), (15) Kirkpatrick et al. (2012), (16) Lawrence et al. (2012), (17) Best et al. (2013), (18) Burningham et al. (2013), (19) Day-Jones et al. (2013), (20) Manjavacas et al. (2013), (21) Mace et al. (2013a), (22) Cutri (2014), (23) Malo et al. (2014), (24) Naud et al. (2014), (25) Best et al. (2015), (26) Gagné et al. (2015), (27) Macintosh et al. (2015), (28) Marocco et al. (2015), (29) Gaia Collaboration et al. (2016), (30) Liu et al. (2016), (31) Magnier et al. (2016), (32) Gagné et al. (2017), (33) Kellogg et al. (2017), (34) Rajan et al. (2017), (35) Vos et al. (2017), (36) Best et al. (2018), (37) Gaia Collaboration et al. (2018), (38) Gagné et al. (2018a), (39) Tinney et al. (2018), (40) Kirkpatrick et al. (2019), (41) Best et al. (2020a), (42) Best et al. (2020b), (43) This Work

Table 2. Photometry of T-Dwarf YMG Members and Candidates

Object	SpT	Near-Infrared MKO Photometry					AllWISE Photometry			*Spitzer*/IRAC Photometry		
		Y_{MKO} (mag)	J_{MKO} (mag)	H_{MKO} (mag)	K_{MKO} (mag)	References	$W1$ (mag)	$W2$ (mag)	References	[3.6] (mag)	[4.5] (mag)	References
AB Doradus												
• New Candidate Members (with trigonometric parallax)												
WISE J163645.56−074325.1	T4.5	17.60 ± 0.05	16.42 ± 0.02	16.28 ± 0.05	16.32 ± 0.05	25,26	15.93 ± 0.06	14.68 ± 0.06	16	–	–	···
WISEPA J062720.07−111428.8	T6	16.37 ± 0.07	15.25 ± 0.05	15.50 ± 0.18	15.51 ± 0.18	26	14.98 ± 0.03	13.25 ± 0.03	16	14.27 ± 0.02	13.32 ± 0.02	9
WISE J233226.49−432510.6	T9	–	19.40 ± 0.10	19.40 ± 0.18	–	10,18	17.97 ± 0.24	14.96 ± 0.07	16	17.27 ± 0.06	15.01 ± 0.02	24
• New Candidate Members (with photometric parallax)												
ULAS J081918.58+210310.4	T6	18.25 ± 0.03	16.954 ± 0.011	17.28 ± 0.04	17.18 ± 0.06	11	16.95 ± 0.11	15.24 ± 0.09	16	–	–	···
• Recovered Previously-Known Members												
2MASS J13243553+6358281	T2.5	16.52 ± 0.08	15.44 ± 0.07	14.68 ± 0.06	14.08 ± 0.06	26	13.12 ± 0.02	12.29 ± 0.02	16	12.56 ± 0.03	12.33 ± 0.03	5
GU Psc b	T3.5	19.40 ± 0.05	18.12 ± 0.03	17.70 ± 0.03	17.40 ± 0.03	17	17.17 ± 0.33	15.41 ± 0.22	17	–	–	···
SDSSp J111010.01+011613.1	T5.5	17.338 ± 0.012	16.161 ± 0.008	16.20 ± 0.02	16.05 ± 0.03	11	15.44 ± 0.04	13.92 ± 0.04	16	–	–	···
Argus												
• New Candidate Members (with trigonometric parallax)												
SDSS J152103.24+013142.7	T3	17.34 ± 0.02	16.097 ± 0.010	15.679 ± 0.009	15.568 ± 0.015	11	14.90 ± 0.03	13.94 ± 0.04	16	–	–	···
2MASS J00132229−1143006	T4	–	16.05 ± 0.02	15.74 ± 0.22	15.76 ± 0.22	25,26	15.49 ± 0.05	14.32 ± 0.05	16	–	–	···
SDSS J020742.48+000056.2	T4.5	18.02 ± 0.03	16.730 ± 0.013	16.81 ± 0.04	16.72 ± 0.05	11	16.30 ± 0.06	15.05 ± 0.07	16	–	–	···
WISE J024124.73−365328.0	T7	–	16.59 ± 0.04	17.04 ± 0.07	–	23,24	16.86 ± 0.08	14.35 ± 0.04	16	15.74 ± 0.03	14.35 ± 0.02	24
• New Candidate Members (with photometric parallax)												
ULAS J004757.41+154641.4	T2	19.12 ± 0.07	17.83 ± 0.05	17.16 ± 0.05	16.42 ± 0.04	11	15.52 ± 0.04	14.86 ± 0.07	16	–	–	···
PSO J168.1800−27.2264	T2.5	18.38 ± 0.04	17.12 ± 0.03	16.75 ± 0.03	16.65 ± 0.06	15,26	15.72 ± 0.05	14.98 ± 0.07	16	–	–	···
ULAS J154701.84+005320.3	T5.5	19.37 ± 0.06	18.32 ± 0.03	18.45 ± 0.07	18.21 ± 0.10	6	16.88 ± 0.10	15.89 ± 0.15	16	–	–	···
ULAS J120744.65+133902.7	T6	19.19 ± 0.05	18.28 ± 0.05	18.52 ± 0.05	18.67 ± 0.05	7	17.90 ± 0.25	15.88 ± 0.14	16	–	–	···
ULAS J075829.83+222526.7	T6.5	18.68 ± 0.04	17.62 ± 0.02	17.91 ± 0.02	17.87 ± 0.12	13	16.52 ± 0.09	15.07 ± 0.08	16	–	–	···
β Pictoris												
• New Candidate Members (with trigonometric parallax)												
WISEPA J081958.05−033529.0	T4	15.94 ± 0.05	14.78 ± 0.02	14.60 ± 0.05	14.64 ± 0.05	25,26	14.35 ± 0.03	13.08 ± 0.03	16	13.61 ± 0.02	13.07 ± 0.02	9
CFBDS J232304.41−015232.3	T6	18.30 ± 0.02	17.23 ± 0.03	17.46 ± 0.04	17.30 ± 0.03	8	16.62 ± 0.09	15.07 ± 0.09	16	–	–	···
WISEPC J225540.74−311841.8	T8	18.38 ± 0.02	17.334 ± 0.011	17.66 ± 0.03	17.42 ± 0.05	20,26	16.55 ± 0.08	14.16 ± 0.05	16	15.91 ± 0.03	14.21 ± 0.02	9
• Recovered Previously-Known Members												
51 Eri b	T6.5	–	19.04 ± 0.40	18.99 ± 0.21	18.67 ± 0.19	22	–	–	···	–	–	···
Carina-Near												
• Newly Confirmed Member												
2MASS J21392676+0220226	T1.5	16.23 ± 0.07	15.10 ± 0.05	14.27 ± 0.05	13.60 ± 0.05	26	12.76 ± 0.02	12.00 ± 0.02	16	–	–	···

Table 2 continued

Table 2 *(continued)*

Object	SpT	Near-Infrared MKO Photometry					AllWISE Photometry			*Spitzer*/IRAC Photometry		
		Y_{MKO} (mag)	J_{MKO} (mag)	H_{MKO} (mag)	K_{MKO} (mag)	References	$W1$ (mag)	$W2$ (mag)	References	[3.6] (mag)	[4.5] (mag)	References
• New Candidate Members (with trigonometric parallax)												
ULAS J131610.13+031205.5	T3	18.00 ± 0.03	16.75 ± 0.02	16.13 ± 0.02	15.43 ± 0.02	11	14.16 ± 0.03	13.76 ± 0.04	16	–	–	···
PSO J004.6359+56.8370	T4.5	–	16.22 ± 0.02	16.24 ± 0.02	16.13 ± 0.02	25	–	–	···	–	–	···
WISE J223617.59+510551.9	T5	15.655 ± 0.014	14.457 ± 0.011	14.61 ± 0.02	14.57 ± 0.05	12,26	13.83 ± 0.03	12.50 ± 0.03	16	–	–	···
SDSSp J162414.37+002915.6	T6	16.28 ± 0.05	15.20 ± 0.05	15.48 ± 0.05	15.61 ± 0.05	1	15.16 ± 0.04	13.09 ± 0.03	16	14.41 ± 0.02	13.10 ± 0.02	24
2MASSI J1553022+153236	T7	16.37 ± 0.06	15.34 ± 0.03	15.76 ± 0.03	15.94 ± 0.03	2	15.29 ± 0.04	13.03 ± 0.03	16	14.51 ± 0.02	13.13 ± 0.02	24
WISE J031624.35+430709.1	T8	–	19.47 ± 0.04	19.70 ± 0.09	–	14	17.79 ± 0.22	14.64 ± 0.05	16	16.64 ± 0.04	14.58 ± 0.02	14
ULAS J130217.21+130851.2	T8.5	19.12 ± 0.03	18.11 ± 0.04	18.60 ± 0.06	18.28 ± 0.03	7	17.69 ± 0.23	14.87 ± 0.07	16	16.510 ± 0.010	14.92 ± 0.02	24
• Recovered Previously-Known Members												
SIMP J013656.5+093347.3	T2.5	14.392 ± 0.003	13.252 ± 0.002	12.809 ± 0.002	12.585 ± 0.002	3,11	11.94 ± 0.02	10.96 ± 0.02	16	–	–	···
Hyades												
• New Candidate Members (with trigonometric parallax)												
PSO J069.7303+04.3834	T2	–	16.39 ± 0.02	15.76 ± 0.02	15.12 ± 0.02	25	14.26 ± 0.03	13.60 ± 0.03	16	–	–	···
PSO J049.1159+26.8409	T2.5	17.17 ± 0.05	16.11 ± 0.02	15.82 ± 0.02	15.50 ± 0.05	19,26	14.98 ± 0.04	13.93 ± 0.04	16	–	–	···
PSO J052.2746+13.3754	T3.5	17.34 ± 0.05	16.23 ± 0.02	15.93 ± 0.05	15.73 ± 0.05	25,26	15.30 ± 0.04	14.26 ± 0.05	16	–	–	···
• New Candidate Members (with photometric parallax)												
WISEPA J030724.57+290447.6	T6.5	18.63 ± 0.06	17.34 ± 0.03	17.75 ± 0.14	18.08 ± 0.12	3,11,26	17.15 ± 0.14	15.06 ± 0.08	16	16.39 ± 0.04	14.97 ± 0.02	9
• Recovered Previously-Known Candidate Members												
CFHT−Hy−20	T2.5	18.11 ± 0.05	17.02 ± 0.05	16.51 ± 0.05	16.08 ± 0.05	4,21	15.60 ± 0.05	14.72 ± 0.08	16	–	–	···
Ursa Major												
• New Candidate Members (with trigonometric parallax)												
SDSS J125011.65+392553.9	T4	–	16.14 ± 0.02	16.24 ± 0.25	16.18 ± 0.25	25,26	15.91 ± 0.05	14.60 ± 0.05	16	–	–	···

References—(1) Strauss et al. (1999), (2) Knapp et al. (2004), (3) Lawrence et al. (2007), (4) Bouvier et al. (2008), (5) Metchev et al. (2008), (6) Pinfield et al. (2008), (7) Burningham et al. (2010a), (8) Albert et al. (2011), (9) Kirkpatrick et al. (2011), (10) Kirkpatrick et al. (2012), (11) Lawrence et al. (2012), (12) Best et al. (2013), (13) Burningham et al. (2013), (14) Mace et al. (2013a), (15) McMahon et al. (2013), (16) Cutri (2014), (17) Naud et al. (2014), (18) Tinney et al. (2014), (19) Best et al. (2015), (20) Edge et al. (2016), (21) Liu et al. (2016), (22) Rajan et al. (2017), (23) Tinney et al. (2018), (24) Kirkpatrick et al. (2019), (25) Best et al. (2020a), (26) Best et al. (2021)

Table 3. Properties of T-Dwarf YMG Members and Candidates

Object	SpT	$\log(L_{\rm bol}/L_\odot)$[a,b] (dex)	Physical Properties[b] $T_{\rm eff}$ (K)	$\log g$ (dex)	R ($R_{\rm Jup}$)	M ($M_{\rm Jup}$)	Peculiarity Photometry[c]	Peculiarity Spectroscopy[d]	Variability[e]
AB Doradus									
• New Candidate Members (with trigonometric parallax)									
WISE J163645.56−074325.1	T4.5	-4.724 ± 0.144	1090^{+94}_{-87}	$4.36^{+0.08}_{-0.06}$	$1.19^{+0.02}_{-0.02}$	$13.1^{+2.2}_{-1.5}$	N	WCC[g]	
WISEPA J062720.07−111428.8	T6	-5.045 ± 0.103	910^{+53}_{-50}	$4.29^{+0.04}_{-0.03}$	$1.178^{+0.011}_{-0.015}$	$11.1^{+0.9}_{-0.7}$	N	N	
WISE J233226.49−432510.6	T9	-6.242 ± 0.040	454^{+11}_{-11}	$3.82^{+0.08}_{-0.05}$	$1.193^{+0.006}_{-0.014}$	$3.8^{+0.7}_{-0.4}$	N	?	
• New Candidate Members (with photometric parallax)									
ULAS J081918.58+210310.4	T6	-5.013 ± 0.158	926^{+84}_{-77}	$4.30^{+0.05}_{-0.04}$	$1.179^{+0.013}_{-0.015}$	$11.2^{+1.2}_{-0.9}$	N	?	
• Recovered Previously-Known Members									
2MASS J13243553+6358281	T2.5	-4.720 ± 0.100	1093^{+65}_{-63}	$4.36^{+0.07}_{-0.05}$	$1.19^{+0.02}_{-0.02}$	$13.2^{+1.8}_{-1.3}$	Red	WCC[f]	$3 \pm 0.3\%$
GU Psc b	T3.5	-4.870 ± 0.100	1002^{+59}_{-54}	$4.32^{+0.05}_{-0.04}$	$1.185^{+0.012}_{-0.015}$	$11.9^{+1.3}_{-0.8}$	N	WCC[f]	$4 \pm 1\%$
SDSSp J111010.01+011613.1	T5.5	-4.970 ± 0.020	948^{+12}_{-11}	$4.30^{+0.04}_{-0.03}$	$1.184^{+0.009}_{-0.015}$	$11.3^{+0.9}_{-0.5}$	N	N	$< 1.25\%$
Argus									
• New Candidate Members (with trigonometric parallax)									
SDSS J152103.24+013142.7	T3	-4.666 ± 0.149	1083^{+91}_{-86}	$4.11^{+0.04}_{-0.04}$	$1.284^{+0.015}_{-0.010}$	$8.5^{+0.9}_{-0.9}$	N	WCC	
2MASS J00132229−1143006	T4	-4.740 ± 0.121	1039^{+71}_{-67}	$4.09^{+0.03}_{-0.04}$	$1.279^{+0.009}_{-0.008}$	$8.1^{+0.7}_{-0.7}$	N	WCC[f,g]	$4.6 \pm 0.2\%$
SDSS J020742.48+000056.2	T4.5	-4.768 ± 0.134	1024^{+78}_{-73}	$4.08^{+0.04}_{-0.04}$	$1.278^{+0.010}_{-0.008}$	$7.9^{+0.8}_{-0.8}$	N	N	
WISE J024124.73−365328.0	T7	-5.312 ± 0.075	754^{+33}_{-31}	$3.90^{+0.03}_{-0.03}$	$1.259^{+0.005}_{-0.005}$	$5.1^{+0.4}_{-0.4}$	N	N	
• New Candidate Members (with photometric parallax)									
ULAS J004757.41+154641.4	T2	-4.710 ± 0.161	1057^{+96}_{-90}	$4.10^{+0.04}_{-0.05}$	$1.281^{+0.013}_{-0.010}$	$8.3^{+0.9}_{-1.0}$	Red	SCC[g]	
PSO J168.1800−27.2264	T2.5	-4.754 ± 0.108	1032^{+63}_{-60}	$4.08^{+0.03}_{-0.04}$	$1.278^{+0.009}_{-0.008}$	$8.0^{+0.7}_{-0.7}$	N	SCC[f]	
ULAS J154701.84+005320.3	T5.5	-5.140 ± 0.170	831^{+83}_{-76}	$3.96^{+0.06}_{-0.07}$	$1.264^{+0.007}_{-0.006}$	$5.9^{+0.9}_{-0.9}$	N	?	
ULAS J120744.65+133902.7	T6	-5.355 ± 0.159	736^{+69}_{-63}	$3.88^{+0.06}_{-0.07}$	$1.258^{+0.006}_{-0.005}$	$4.9^{+0.8}_{-0.7}$	N	?	
ULAS J075829.83+222526.7	T6.5	-5.375 ± 0.163	727^{+70}_{-64}	$3.87^{+0.06}_{-0.07}$	$1.258^{+0.006}_{-0.005}$	$4.8^{+0.8}_{-0.7}$	N	?	
β Pictoris									
• New Candidate Members (with trigonometric parallax)									
WISEPA J081958.05−033529.0	T4	-4.769 ± 0.078	1004^{+44}_{-42}	$3.91^{+0.04}_{-0.04}$	$1.325^{+0.011}_{-0.010}$	$5.7^{+0.5}_{-0.5}$	N	WCC	
CFBDS J232304.41−015232.3	T6	-4.979 ± 0.147	894^{+75}_{-70}	$3.84^{+0.06}_{-0.06}$	$1.311^{+0.013}_{-0.010}$	$4.8^{+0.7}_{-0.7}$	N	?	
WISEPC J225540.74−311841.8	T8	-5.787 ± 0.057	577^{+16}_{-14}	$3.54^{+0.03}_{-0.02}$	$1.274^{+0.005}_{-0.005}$	$2.3^{+0.2}_{-0.1}$	Red	N	
• Recovered Previously-Known Members									
51 Eri b	T6.5	-5.870 ± 0.150	588^{+35}_{-25}	$3.55^{+0.05}_{-0.03}$	$1.276^{+0.007}_{-0.006}$	$2.3^{+0.3}_{-0.2}$	Red+Faint	N	
Carina-Near									
• Newly Confirmed Member									
2MASS J21392676+0220226	T1.5	-4.710 ± 0.056	1111^{+37}_{-42}	$4.42^{+0.12}_{-0.06}$	$1.17^{+0.02}_{-0.04}$	$14.6^{+3.2}_{-1.6}$	Red+Faint	WCC[f,g]	$26 \pm 1\%$

Table 3 continued

Table 3 *(continued)*

Object	SpT	$\log(L_{\rm bol}/L_{\odot})$[a,b] (dex)	Physical Properties[b] $T_{\rm eff}$ (K)	$\log g$ (dex)	R ($R_{\rm Jup}$)	M ($M_{\rm Jup}$)	Peculiarity Photometry[c]	Spectroscopy[d]	Variability[e]
• New Candidate Members (with trigonometric parallax)									
ULAS J131610.13+031205.5	T3	-4.431 ± 0.131	1284^{+113}_{-77}	$4.57^{+0.18}_{-0.16}$	$1.17^{+0.05}_{-0.04}$	$20.3^{+9.1}_{-5.0}$	Red	SCC[g]	
PSO J004.6359+56.8370	T4.5	-4.956 ± 0.093	960^{+51}_{-47}	$4.35^{+0.06}_{-0.05}$	$1.170^{+0.014}_{-0.021}$	$12.3^{+1.4}_{-1.0}$	N	N	
WISE J223617.59+510551.9	T5	-4.975 ± 0.069	950^{+41}_{-35}	$4.34^{+0.06}_{-0.04}$	$1.17^{+0.02}_{-0.02}$	$12.1^{+1.3}_{-0.9}$	N	N	
SDSSp J162414.37+002915.6	T6	-5.238 ± 0.062	820^{+30}_{-29}	$4.31^{+0.04}_{-0.05}$	$1.156^{+0.016}_{-0.013}$	$11.0^{+0.8}_{-1.0}$	N	N	
2MASSI J1553022+153236	T7	-5.021 ± 0.093	927^{+50}_{-47}	$4.34^{+0.06}_{-0.04}$	$1.17^{+0.02}_{-0.02}$	$12.0^{+1.3}_{-1.0}$	N	N	
WISE J031624.35+430709.1	T8	-6.180 ± 0.038	473^{+11}_{-11}	$3.93^{+0.07}_{-0.08}$	$1.178^{+0.015}_{-0.013}$	$4.8^{+0.7}_{-0.7}$	Faint	?	
ULAS J130217.21+130851.2	T8.5	-6.035 ± 0.077	514^{+24}_{-23}	$4.00^{+0.08}_{-0.09}$	$1.175^{+0.017}_{-0.015}$	$5.6^{+0.9}_{-0.9}$	Red	?	
• Recovered Previously-Known Members									
SIMP J013656.5+093347.3	T2.5	-4.688 ± 0.005	1126^{+16}_{-15}	$4.46^{+0.09}_{-0.08}$	$1.16^{+0.03}_{-0.03}$	$15.6^{+2.4}_{-2.1}$	N	WCC	$\approx 5\%$
Hyades									
• New Candidate Members (with trigonometric parallax)									
PSO J069.7303+04.3834	T2	-4.390 ± 0.160	1445^{+147}_{-135}	$5.10^{+0.08}_{-0.13}$	$0.99^{+0.02}_{-0.02}$	$50.0^{+7.7}_{-11.9}$	Red	SCC[g]	
PSO J049.1159+26.8409	T2.5	-4.521 ± 0.096	1331^{+83}_{-72}	$5.00^{+0.10}_{-0.09}$	$1.00^{+0.02}_{-0.02}$	$40.6^{+8.5}_{-7.1}$	Bright	SCC[f,g]	
PSO J052.2746+13.3754	T3.5	-4.770 ± 0.136	1154^{+94}_{-88}	$4.86^{+0.07}_{-0.05}$	$1.003^{+0.015}_{-0.014}$	$29.6^{+4.3}_{-2.9}$	N	N	
• New Candidate Members (with photometric parallax)									
WISEPA J030724.57+290447.6	T6.5	-5.480 ± 0.123	755^{+59}_{-55}	$4.63^{+0.06}_{-0.09}$	$1.03^{+0.02}_{-0.02}$	$18.4^{+2.3}_{-2.7}$	N	?	
• Recovered Previously-Known Candidate Members									
CFHT−Hy−20	T2.5	-4.663 ± 0.071	1220^{+41}_{-40}	$4.90^{+0.05}_{-0.05}$	$1.003^{+0.015}_{-0.014}$	$32.0^{+3.1}_{-2.6}$	N	WCC	
Ursa Major									
• New Candidate Members (with trigonometric parallax)									
SDSS J125011.65+392553.9	T4	-4.909 ± 0.128	1023^{+88}_{-79}	$4.65^{+0.14}_{-0.29}$	$1.07^{+0.10}_{-0.05}$	$20.6^{+5.2}_{-8.0}$	N	?	

[a] Bolometric luminosities for our candidate members with photometric parallaxes should be used with caution.

[b] Bolometric luminosities and physical properties of previously-known YMG members and candidate members are from Table 4 of Zhang et al. (2020a).

[c] Objects with "Red" have much redder $J-K$ colors than field dwarfs with similar spectral types, and those with "Faint" or "Bright" have much fainter or brighter J-band absolute magnitudes than the field sequence (see Figure 2).

[d] Objects with "SCC" and "WCC" are strong and weak composite candidates, respectively, based on the Burgasser et al. (2010a) and Bardalez Gagliuffi et al. (2015) criteria (see Section 3.2). We use "?" for objects whose spectra have only partial wavelength coverage in the near-infrared and/or have not been vetted for spectral peculiarity by previous work. We use "N" for objects with normal spectra.

[e] We provide peak-to-peak amplitudes in J band for variable ultracool dwarfs 2MASS J00132229 − 1143006 (Eriksson et al. 2019b), 2MASS J21392676 + 0220226 (Radigan et al. 2012), GU Psc b (Naud et al. 2017b), and SIMP J013656.5 + 093347.3 (Artigau et al. 2009; Radigan et al. 2014; Vos et al. 2017), and in *Spitzer*/IRAC [4.5] band for SDSSp J111010.01 + 011613.1 (Vos et al. 2018) and 2MASS J13243559 + 6358284 (Metchev et al. 2015).

[f] Potential binarity of our 4 YMG candidates and 2 previously-known YMG members have been previously noted by using the same quantitative spectral indices as in this work: 2MASS J21392676 + 0220226 and 2MASS J13243553 + 6358281 by Burgasser et al. (2010a), GU Psc b by Naud et al. (2014), PSO J049.1159 + 26.8409 and PSO J168.1800 − 27.2264 by Best et al. (2015), and 2MASS J00132229 − 1143006 by Kellogg et al. (2017).

[g] These 7 objects have peculiar spectra indicative of either atmospheric variability or unresolved binarity (Section 3.2).

Table 4. T7−Y1 Benchmarks: Spectral Type, Photometry, Parallax, and Age

Object	SpT	MKO Photometry				Parallax	Age	Primary SpT	Separation	References				
		Y_{MKO} (mag)	J_{MKO} (mag)	H_{MKO} (mag)	K_{MKO} (mag)	(mas)	(Gyr)		($''$)	Discovery	SpT	Phot.	π	Age
Gl 229B	T7 pec	15.17 ± 0.10	14.01 ± 0.05	14.36 ± 0.05	14.36 ± 0.05	173.70 ± 0.05	$8.6^{+1.4}_{-0.6}$	M1V	7.8	1	4	3	30,34	37
HD 3651B	T7.5	17.12 ± 0.06	16.16 ± 0.03	16.68 ± 0.04	16.87 ± 0.05	89.79 ± 0.06	$4.5 - 8.3$	K0V	42.9	5	6	6,41	30,34	40
ULAS J141623.94+134836.3	sd T7.5	18.16 ± 0.03	17.26 ± 0.02	17.58 ± 0.03	18.42 ± 0.09	107.56 ± 0.30	$0.5 - 10$	sd L7	9.8	11,15	10	19,41	30,34	28
GJ 570D	T7.5	15.78 ± 0.10	14.82 ± 0.05	15.28 ± 0.05	15.52 ± 0.05	170.01 ± 0.09	$1.4 - 5.2$	K4V + M1.5V + M3V	258.3	2	4	14	30,34	40
ULAS J095047.28+011734.3	T8	18.90 ± 0.03	18.02 ± 0.03	18.40 ± 0.03	18.85 ± 0.07	50.80 ± 0.08	> 3.5	M4V	52.0	22	26	22	30,34	22
Ross 458C	T8	17.72 ± 0.03	16.69 ± 0.01	17.01 ± 0.04	16.90 ± 0.06	86.86 ± 0.15	$0.15 - 0.8$	M0.5V + M7V	103.0	13	16	19	30,34	12
BD +01° 2920B	T8	19.51 ± 0.14	18.55 ± 0.03	18.96 ± 0.07	19.89 ± 0.33	58.20 ± 0.50	$2.3 - 14.4$	G1V	153.0	21	26	19,21,26	7	21
WISEU J005559.88+594745.0	T8	–	17.90 ± 0.05	–	–	43.78 ± 0.07	10 ± 3	DC	17.6	39	39	39	30,34	39
WISEU J215018.99−752054.6	T8	18.53 ± 0.13	18.10 ± 0.10	–	–	41.36 ± 0.28	$0.5 - 10$	L1	14.1	38	38	39	30,34	38
Wolf 1130C	sd T8	–	19.64 ± 0.09	19.57 ± 0.08	–	60.39 ± 0.03	> 10	sdM1 + WD	188.5	25	25	25	30,34	35
WISE J111838.70+312537.9	T8.5	19.18 ± 0.12	17.79 ± 0.05	18.15 ± 0.06	18.75 ± 0.15	114.50 ± 0.40	> 2	F8.5V + G2V[a]	510.0	27	27	27	30,34	27
Wolf 940B	T8.5	18.97 ± 0.03	18.16 ± 0.02	18.77 ± 0.03	18.85 ± 0.05	80.77 ± 0.11	$3.5 - 6.0$	dM4	32.0	8	8	8	30,34	8
Gl 758B	T5−T8	–	18.57 ± 0.20	19.15 ± 0.20	–	64.06 ± 0.02	8.8 ± 0.9	K0V	1.9	9	33	17	30,34	42
GJ 504 b	late-T	–	19.76 ± 0.10	19.99 ± 0.10	19.38 ± 0.11	57.02 ± 0.25	$0.1 - 6.5$	G0V	2.5	24	24	23	30,34	31
WD 0806−661B	Y1	–	25.00 ± 0.10	25.29 ± 0.14	–	51.93 ± 0.02	2 ± 0.5	DQ	130.2	18	36	29,32	30,34	20

[a] The two primary stars of WISE J111838.70 + 312537.9 form a gravitationally bound binary system (Herschel 1804) and are both spectroscopic binaries (e.g., Heintz 1967).

References—(1) Nakajima et al. (1995), (2) Burgasser et al. (2000), (3) Leggett et al. (2002), (4) Burgasser et al. (2006), (5) Mugrauer et al. (2006), (6) Luhman et al. (2007), (7) van Leeuwen (2007), (8) Burningham et al. (2009), (9) Thalmann et al. (2009), (10) Burgasser et al. (2010b), (11) Burningham et al. (2010b), (12) Burgasser et al. (2010c), (13) Goldman et al. (2010), (14) Leggett et al. (2010), (15) Scholz (2010), (16) Cushing et al. (2011), (17) Janson et al. (2011), (18) Luhman et al. (2011), (19) Lawrence et al. (2012), (20) Luhman et al. (2012), (21) Pinfield et al. (2012), (22) Burningham et al. (2013), (23) Janson et al. (2013), (24) Kuzuhara et al. (2013), (25) Mace et al. (2013b), (26) Mace et al. (2013a), (27) Wright et al. (2013), (28) Filippazzo et al. (2015), (29) Leggett et al. (2015), (30) Gaia Collaboration et al. (2016), (31) Skemer et al. (2016), (32) Leggett et al. (2017), (33) Nilsson et al. (2017), (34) Gaia Collaboration et al. (2018), (35) Mace et al. (2018), (36) Kirkpatrick et al. (2019), (37) Brandt et al. (2020), (38) Faherty et al. (2020), (39) Meisner et al. (2020), (40) Zhang et al. (2020b), (41) Best et al. (2021), (42) This Work

Table 5. T7−Y1 Benchmarks: Bolometric Luminosity, Effective Temperature, Surface Gravity, Radius, and Mass

Object	SpT	$\log(L_{\rm bol}/L_\odot)$	Physical Properties[b]				References	
			$T_{\rm eff}$	$\log g$	R	M	$L_{\rm bol}$	Phys.
		(dex)	(K)	(dex)	($R_{\rm Jup}$)	($M_{\rm Jup}$)		
Gl 229B	T7 pec	-5.208 ± 0.007	1011^{+6}_{-5}	$5.40^{+0.02}_{-0.01}$	$0.79^{+0.00}_{-0.01}$	$70.0^{+5.0}_{-5.0}$[a]	4	8
HD 3651B	T7.5	-5.57 ± 0.03	802^{+17}_{-17}	$5.24^{+0.05}_{-0.07}$	$0.83^{+0.02}_{-0.02}$	$47.8^{+4.0}_{-4.6}$	10	11
ULAS J141623.94+134836.3	sd T7.5	-5.79 ± 0.01	691^{+19}_{-36}	$5.09^{+0.15}_{-0.29}$	$0.87^{+0.10}_{-0.05}$	$37.4^{+9.4}_{-14.0}$	4	11
GJ 570D	T7.5	-5.54 ± 0.03	786^{+21}_{-23}	$5.06^{+0.10}_{-0.15}$	$0.89^{+0.05}_{-0.03}$	$36.2^{+5.8}_{-7.6}$	10	11
ULAS J095047.28+011734.3	T8	-5.63 ± 0.07	774^{+36}_{-36}	$5.23^{+0.08}_{-0.12}$	$0.83^{+0.04}_{-0.03}$	$47.0^{+6.4}_{-7.8}$	3	11
Ross 458C	T8	$-5.60^{+0.03}_{-0.04}$	683^{+18}_{-19}	$4.41^{+0.13}_{-0.15}$	$1.10^{+0.04}_{-0.04}$	$12.5^{+3.2}_{-2.8}$	10	11
BD +01° 2920B	T8	-5.83 ± 0.05	677^{+27}_{-27}	$5.12^{+0.11}_{-0.17}$	$0.85^{+0.06}_{-0.03}$	$39.0^{+7.1}_{-9.1}$	2	11
WISEU J005559.88+594745.0[b]	T8	-5.712 ± 0.008	753	5.317	0.7955	53.1	11	11
WISEU J215018.99−752054.6	T8	-5.64 ± 0.02	758^{+23}_{-39}	$5.15^{+0.14}_{-0.29}$	$0.85^{+0.10}_{-0.05}$	$41.7^{+10.1}_{-15.1}$	9	11
Wolf 1130C[b]	sd T8	-5.949 ± 0.007	647	5.219	0.8189	44.9	11	11
WISE J111838.70+312537.9	T8.5	-6.063 ± 0.008	584^{+13}_{-19}	$5.01^{+0.12}_{-0.19}$	$0.88^{+0.06}_{-0.04}$	$31.9^{+6.4}_{-8.3}$	11	11
Wolf 940B	T8.5	-6.07 ± 0.04	574^{+16}_{-16}	$4.93^{+0.05}_{-0.06}$	$0.91^{+0.02}_{-0.02}$	$28.2^{+2.6}_{-2.7}$	1	11
Gl 758B	T5−T8	-6.07 ± 0.03	594^{+10}_{-10}	$5.12^{+0.03}_{-0.03}$	$0.85^{+0.01}_{-0.01}$	$37.9^{+1.5}_{-1.5}$[a]	6	7,11
GJ 504 b	late-T	-6.13 ± 0.03	540^{+18}_{-28}	$4.79^{+0.15}_{-0.36}$	$0.95^{+0.11}_{-0.05}$	$22.3^{+6.3}_{-10.2}$	5	11
WD 0806−661B	Y1	-6.983 ± 0.017	328^{+4}_{-4}	$4.22^{+0.07}_{-0.09}$	$1.07^{+0.02}_{-0.02}$	$7.8^{+1.0}_{-1.2}$	11	11

[a] Directly measured dynamical masses of Gl 229B and Gl 758B are listed in the table and their estimated masses from the Saumon & Marley (2008) hybrid evolutionary models (using their dynamical masses as the prior and their measured $L_{\rm bol}$) are $63.1^{+1.7}_{-0.9}$ $M_{\rm Jup}$ (Brandt et al. 2020) and 38.1 ± 1.7 $M_{\rm Jup}$ (Section 3.3), respectively.

[b] Physical properties of WISEU J005559.88+594745.0 and Wolf 1130C are derived by assuming an age of 10 Gyr. Only median values of these two objects' properties are shown here, with uncertainties of 4 K in $T_{\rm eff}$, 0.003 dex in $\log g$, 8×10^{-4} $R_{\rm Jup}$ in R, and 0.3 $M_{\rm Jup}$ in M for both objects.

References—(1) Burningham et al. (2009), (2) Pinfield et al. (2012), (3) Burningham et al. (2013), (4) Filippazzo et al. (2015), (5) Skemer et al. (2016), (6) Bowler et al. (2018), (7) Brandt et al. (2019), (8) Brandt et al. (2020), (9) Faherty et al. (2020), (10) Zhang et al. (2020b), (11) This Work